© 2019. Published by The Company of Biologists Ltd | Biology Open (2019) 8, bio039800. doi:10.1242/bio.039800

RESEARCH ARTICLE

The Forkhead box F1 transcription factor inhibits collagen deposition and accumulation of myofibroblasts during liver fibrosis

Hannah M. Flood[1], Craig Bolte[1], Nupur Dasgupta[2], Akanksha Sharma[3], Yufang Zhang[1], Chandrashekhar R. Gandhi[1,3], Tanya V. Kalin[1] and Vladimir V. Kalinichenko[1,*]

ABSTRACT

Hepatic fibrosis is the common end stage to a variety of chronic liver injuries and is characterized by an excessive deposition of extracellular matrix (ECM), which disrupts the liver architecture and impairs liver function. The fibrous lesions are produced by myofibroblasts, which differentiate from hepatic stellate cells (HSC). The myofibroblast's transcriptional networks remain poorly characterized. Previous studies have shown that the Forkhead box F1 (FOXF1) transcription factor is expressed in HSCs and stimulates their activation during acute liver injury; however, the role of FOXF1 in the progression of hepatic fibrosis is unknown. In the present study, we generated *αSMACreER;Foxf1$^{fl/fl}$* mice to conditionally inactivate *Foxf1* in myofibroblasts during carbon tetrachloride-mediated liver fibrosis. *Foxf1* deletion increased collagen depositions and disrupted liver architecture. *Timp2* expression was significantly increased in *Foxf1*-deficient mice while MMP9 activity was reduced. RNA sequencing of purified liver myofibroblasts demonstrated that FOXF1 inhibits expression of pro-fibrotic genes, *Col1α2*, *Col5α2*, and *Mmp2* in fibrotic livers and binds to active repressors located in promotors and introns of these genes. Overexpression of FOXF1 inhibits *Col1a2*, *Col5a2*, and *MMP2* in primary murine HSCs *in vitro*. Altogether, FOXF1 prevents aberrant ECM depositions during hepatic fibrosis by repressing pro-fibrotic gene transcription in myofibroblasts and HSCs.

KEY WORDS: FOXF1, Hepatic fibrosis, Myofibroblast, Hepatic stellate cell, Carbon tetrachloride liver injury

INTRODUCTION

The liver is the body's filter and insults can result from a variety of infectious, toxic and metabolic agents. Hepatic fibrosis is the common end stage to a multitude of liver diseases (Civan, 2016) and is characterized by an excessive deposition of extracellular matrix (ECM) and collagen (Cheng and Mahato, 2007). Novel animal models of hepatic fibrosis are greatly needed to identify molecular mechanisms responsible for the disease pathogenesis and for the development of therapeutic agents. Hepatic stellate cells (HSC) reside in the space of Disse and are characterized by their storage of lipids when in the quiescent state (Yin et al., 2013; Croci et al., 2013). During fibrogenesis, quiescent HSCs differentiate into myofibroblasts (MF) in response to cytokine signaling from damaged hepatocytes and immune cells after liver insult. MFs secrete ECM and collagen to encapsulate the site of injury and shield the liver from plaguing insults (Cheng and Mahato, 2007). While HSCs and MFs make up only a small number of cells in liver tissue, they are the main contributors of ECM and collagen during liver repair and fibrogenesis (Brenner et al., 2012; Fausther et al., 2013). The TGF-β and PDGF signaling pathways play key roles in hepatic fibrosis and HSC activation (Makarev et al., 2016). TGF-β signaling stimulates cellular transdifferentiation of HSCs to MFs (Hellerbrand et al., 1999; Bachem et al., 1993), whereas PDGF signaling induces cellular proliferation in fibrotic foci (Wong et al., 1994; Kinnman et al., 2002).

The Forkhead Box F1 (FOXF1) transcription factor is expressed in human and murine HSCs and is important in regulating stellate cell activation after acute liver injury (Kalinichenko et al., 2003). In the advanced disease state of hepatocellular carcinoma (HCC), which is associated with significant fibrotic depositions, *FOXF1* expression has been shown to be significantly decreased (Hodo et al., 2013). *Foxf1*$^{-/-}$ mice are embryonic lethal due to severe developmental abnormalities in the yolk sac and allantois (Mahlapuu et al., 2001). Murine haploinsufficiency of *Foxf1* causes lung hypoplasia, loss of alveolar capillaries in the lung and gall bladder agenesis (Kalinichenko et al., 2002; Bolte et al., 2018), and was associated with delayed lung and liver repair. After acute liver injury by carbon tetrachloride (CCl_4), *Foxf1*$^{+/-}$ mice exhibited diminished activation of HSCs and delayed liver repair, indicating that FOXF1 is essential for liver repair after acute liver injury (Kalinichenko et al., 2003). *Foxf1* siRNA delivered to mice through nanoparticles prevented activation of HSCs and subsequent collagen deposition after cholestatic liver injury (Abshagen et al., 2015). While these studies have shown that FOXF1 is required for activation of HSCs after acute liver injury, the role of FOXF1 in MFs and in the progression of fibrotic responses remains unknown.

In the present study, we generated a novel genetic mouse model to conditionally delete *Foxf1* from MFs (*αSMACreER;Foxf1$^{fl/fl}$*). During chronic liver injury, deletion of *Foxf1* in MFs exacerbated hepatic fibrosis, increased collagen deposition and stimulated expression of profibrotic genes in the liver tissue. Our studies indicate that *Foxf1* expression in MFs is critical to prevent MF accumulation and collagen deposition during liver fibrosis.

RESULTS

Deletion of *Foxf1* in αSMA-positive cells exacerbates CCl_4-induced hepatic fibrosis

Previous studies demonstrated that FOXF1 is present in HSCs in murine developing and adult livers (Kalinichenko et al., 2003; Kim et al., 2005). Consistent with these studies, FOXF1 staining was

[1]Department of Pediatrics, Cincinnati Children's Research Foundation, Cincinnati, Ohio 45229, USA. [2]Division of Human Genetics, Cincinnati Children's Research Foundation, Cincinnati, Ohio 45229, USA. [3]Division of Gastroenterology, Hepatology, and Nutrition, Cincinnati Children's Research Foundation, Cincinnati, Ohio 45229, USA.

*Author for correspondence (Vladimir.Kalinichenko@cchmc.org)

V.V.K., 0000-0003-3438-2660

Received 30 October 2018; Accepted 14 January 2019

Biology Open (2019) 8, bio039800. doi:10.1242/bio.039800

detected in livers of e12.5-e17.5 mouse embryos as well as in mesenchyme of stomach and intestine (Fig. S1). In adult mice, FOXF1 is specifically expressed in the liver parenchyma but not in endothelial or smooth muscle cells surrounding the portal vein or hepatic artery (Kalinichenko et al., 2003) (Fig. 1A; Fig. S1), and FOXF1 staining co-localized with desmin (DES) (Fig. 1A), a known marker of HSCs (Yokoi et al., 1984). To investigate the role of *Foxf1* in liver fibrosis, we utilized a conditional knockout approach. Transgenic mice containing a tamoxifen-inducible *αSMA-CreER* transgene and two *Foxf1*-floxed alleles (*αSMACreER;Foxf1*$^{fl/fl}$) were generated by breeding *αSMA-CreER* and *Foxf1*$^{fl/fl}$ mice (Fig. 1B,C). Hepatic fibrosis was induced by chronic liver injury using multiple administrations of CCl_4, which is known to increase fibrotic depositions and disrupt liver architecture in experimental mice (Martinez et al., 2014). Tamoxifen was given three times per week to achieve a continuous deletion of *Foxf1* in αSMA-positive MFs (Fig. 1D) that derive from HSCs after liver injury (Mederacke et al., 2013). Morphological analysis of liver sections revealed increased fibrotic deposition in CCl_4-treated *αSMACreER;Foxf1*$^{-/-}$ livers compared to controls as shown by H&E (Fig. 1E; Fig. S2) and Masson's Trichrome staining (Fig. 1F; Fig. S2). Increased fibrosis in *αSMACreER;Foxf1*$^{-/-}$ livers was confirmed by significant increases in collagen levels by Sircol (Fig. 1G) and hydroxyproline (Fig. S2) assays as well as by qRT-PCR for *Col1α1* and *Col3α1* mRNAs (Fig. 1H). Treatment with tamoxifen alone (without CCl_4) did not affect liver architecture or induce liver fibrosis (Fig. S2). Thus, deletion of *Foxf1* from MFs accelerates liver fibrosis after chronic liver injury.

FOXF1 expression is decreased in hepatic myofibroblasts of *αSMACreER;Foxf1*$^{-/-}$ mice

Since FOXF1 is expressed in HSCs in the liver (Kalinichenko et al., 2003), we examined the efficiency of *Foxf1* deletion in our experimental model, using immunostaining for FOXF1 and DES. Without CCl_4 treatment, FOXF1 was observed in cell nuclei of DES-positive stellate cells in *Foxf1*$^{fl/fl}$ and *αSMACreER;Foxf1*$^{fl/fl}$ livers (Fig. 2A). After CCl_4 and Tam treatment, FOXF1 staining was reduced in DES-positive cells of *αSMACreER;Foxf1*$^{-/-}$ livers but not in *Foxf1*$^{fl/fl}$ livers (Fig. 2A). We also immunostained liver sections for FOXF1 and αSMA, a marker of MFs (Rockey et al., 2013). While αSMA was not detected in parenchyma of quiescent livers, αSMA staining was increased after CCl_4 injury. FOXF1 was detected in MFs of control livers but not in *αSMACreER;Foxf1*$^{-/-}$ livers (Fig. 2B). Quantitative counts of FOXF1-expressing cells demonstrated that the number and percentage of FOXF1$^+$ MFs (FOXF1$^+$ αSMA$^+$) were reduced whereas the number and percentage of FOXF1$^-$ MFs (FOXF1$^-$ αSMA$^+$) were elevated in injured *αSMACreER;Foxf1*$^{-/-}$ livers compared to controls (Fig. S3).

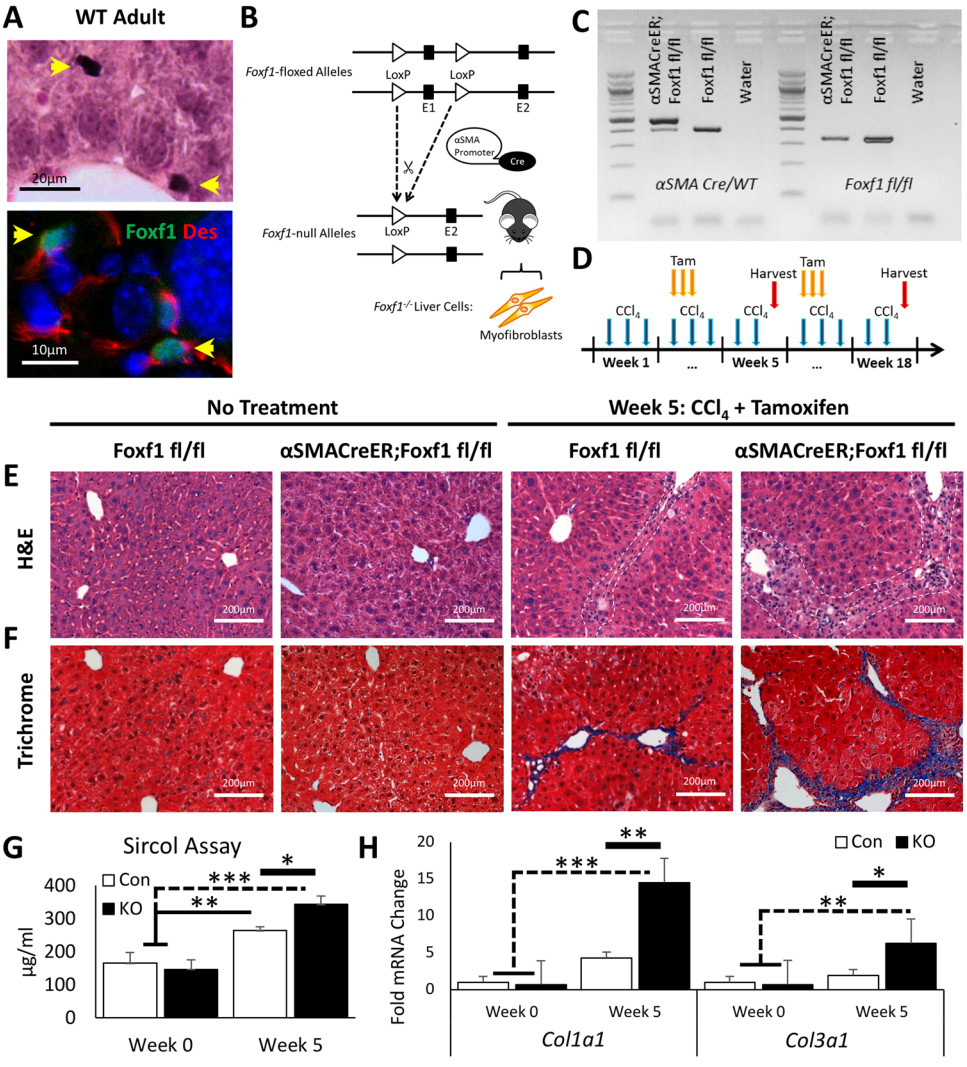

Fig. 1. Hepatic fibrosis is increased after CCl_4 injury in mice with FOXF1 deficiency. (A) FOXF1 co-localizes with DES in hepatic stellate cells in adult mice. (B) Diagram demonstrates *αSMA-CreER* transgene with LoxP sites flanking the *Foxf1* Exon 1 (encoding DNA-binding domain). (C) DNA gel shows genotypes of *Foxf1*$^{fl/fl}$ and *αSMACreER;Foxf1*$^{fl/fl}$ mice. (D) Diagram illustrates CCl_4 and tamoxifen (Tam) treatment protocol. (E,F) H&E and Masson's trichrome staining show fibrotic depositions after five weeks of CCl_4 treatment. Fibrosis was increased in livers from *αSMACreER;Foxf1*$^{-/-}$ mice. White dashed lines indicate fibrotic lesion boundaries. (G) Collagen deposition was quantitated using the Sircol assay. *n*=2 mice per group in week 0; *n*=4 mice per group in week 5. (H) qRT-PCR analysis demonstrates significant increases in *Col1α1* and *Col3α1* mRNAs in livers from *αSMACreER;Foxf1*$^{-/-}$ mice. *n*=3 mice per group in week 0; *n*=5 mice per group in week 5. Untreated livers from *Foxf1*$^{fl/fl}$ and *αSMACreER;Foxf1*$^{fl/fl}$ mice were used as normal controls. mRNAs were normalized to *Actb*. **P*<0.05, ***P*<0.01, ****P*<0.001.

Biology Open (2019) 8, bio039800. doi:10.1242/bio.039800

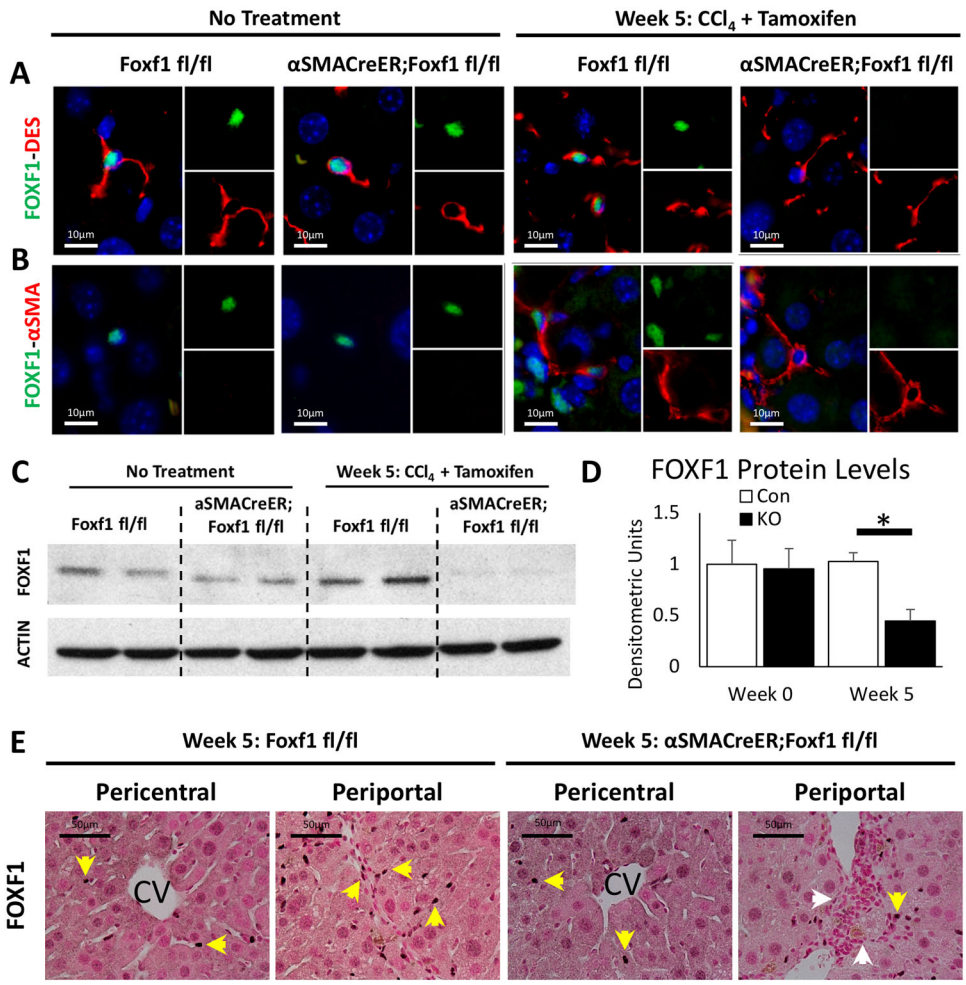

Fig. 2. αSMA-CreER effectively deletes *Foxf1* from hepatic myofibroblasts. (A,B) FOXF1 co-localizes with DES in HSCs before and after CCl_4-induced injury. FOXF1 co-localizes with DES and αSMA in MFs after chronic liver injury. *αSMA-CreER* effectively deletes *Foxf1* from MFs after Tam treatment. (C) Western blot shows total liver protein levels of FOXF1 are decreased in *αSMACreER;Foxf1*$^{-/-}$ livers after CCl_4 injury. Cropped blots are presented here with full length blots presented in Fig. S12. (D) Quantification of western blot revealed a significant loss of FOXF1 in *αSMACreER;Foxf1*$^{-/-}$ livers. Quantification was averaged across four blots. FOXF1 levels were internally normalized to ACTIN for each sample. **P*<0.05. (E) FOXF1 staining is detected in liver parenchyma and fibrotic regions (yellow arrows). FOXF1 staining is decreased in fibrotic regions of *αSMACreER;Foxf1*$^{-/-}$ livers (white arrows).

FOXF1 protein and mRNA were increased in CCl_4-treated *Foxf1*$^{fl/fl}$ livers and purified HSCs (Fig. 2C,D; Fig. S3) but not in the *αSMACreER;Foxf1*$^{-/-}$ livers (Fig. 2C,D). The loss of FOXF1 in *αSMACreER;Foxf1*$^{-/-}$ livers occurred in periportal regions while pericentral regions were unaffected (Fig. 2E). The *αSMA-CreER* transgene allows for the maintained presence of FOXF1 for HSC activation (Kalinichenko et al., 2003) and only deletes FOXF1 after *αSMA* is expressed in MFs. Thus, *αSMA-CreER* transgene effectively deletes *Foxf1* from hepatic MFs during CCl_4-mediated chronic liver injury.

Deletion of *Foxf1* reduces MMP9 activity in CCl_4-injured livers

Histological staining with Sirius Red/Fast Green showed a significant increase in collagen accumulation in *αSMACreER;Foxf1*$^{-/-}$ livers after five weeks of CCl_4 treatment (Fig. 3A; Fig. S4). Increased fibrosis in *Foxf1*-deficient livers was confirmed by immunostaining for DES and αSMA (Fig. 3B,C). To examine the consequences of extended CCl_4 treatment, we treated mice with CCl_4 for 18 weeks. While hepatic enzymes AST and ALT were increased in blood serum after 18 weeks of CCl_4, there was no difference between CCl_4 treated *αSMACreER;Foxf1*$^{-/-}$ and control mice (Fig. 3D,E). Blood serum protein (albumin, globulin) and bilirubin (direct, indirect) levels were not affected after deletion of *Foxf1* (Fig. S5). Collagen accumulation was time-dependent (Fig. S6), and after 18 weeks of CCl_4 treatment, resulted in widespread liver fibrosis (Fig. S7) and in rare cases, the appearance of visible tumors (Fig. S7).

Since MMP9 plays an important role in collagen degradation after liver injury (Duarte et al., 2015), we evaluated mRNA expression of *Mmp9* and its inhibitor, *Timp2*, in liver tissue. *Timp2* mRNA was increased in CCl_4-injured *αSMACreER;Foxf1*$^{-/-}$ livers compared to controls (Fig. 3F). Although *Mmp9* mRNA was unchanged (Fig. S8), evaluation of MMP9 activity through zymography demonstrated a significant decrease in enzymatic activity of MMP9 in *αSMACreER;Foxf1*$^{-/-}$ livers after CCl_4 treatment (Fig. 3G,H). *Mmp8*, *Mmp13*, *Mmp16*, *Timp1* and *Timp3* mRNA levels were not affected in *Foxf1*-deficient livers (Fig. S8). Thus, *Foxf1* deletion from MFs increases *Timp2* mRNA and reduces MMP9 activity in fibrotic livers.

Deletion of *Foxf1* does not influence cellular proliferation in fibrotic livers

We evaluated proliferation markers to investigate if the increased fibrosis in *αSMACreER;Foxf1*$^{-/-}$ livers was due to an expansion of the stromal cells. While cellular proliferation was increased after CCl_4 treatment, there were no significant differences in the number of proliferating hepatocytes or non-hepatocytes between *Foxf1*$^{fl/fl}$ and *αSMACreER;Foxf1*$^{-/-}$ livers (Fig. 4A–C; Fig. S9). Hepatocytes and non-hepatocytes were identified through distinct morphological appearances (Malarkey et al., 2005) from high magnification images. mRNAs of proliferation-specific genes *Foxm1*, *Ccnb1*, *Ccnd1*, and *AurKB* (Wang et al., 2009; Kalin et al., 2011; Ren et al., 2013) were unchanged between *Foxf1*$^{fl/fl}$ and *αSMACreER;Foxf1*$^{-/-}$ livers (Fig. 4D). Proliferating HSCs and MFs were detected in

Biology Open (2019) 8, bio039800. doi:10.1242/bio.039800

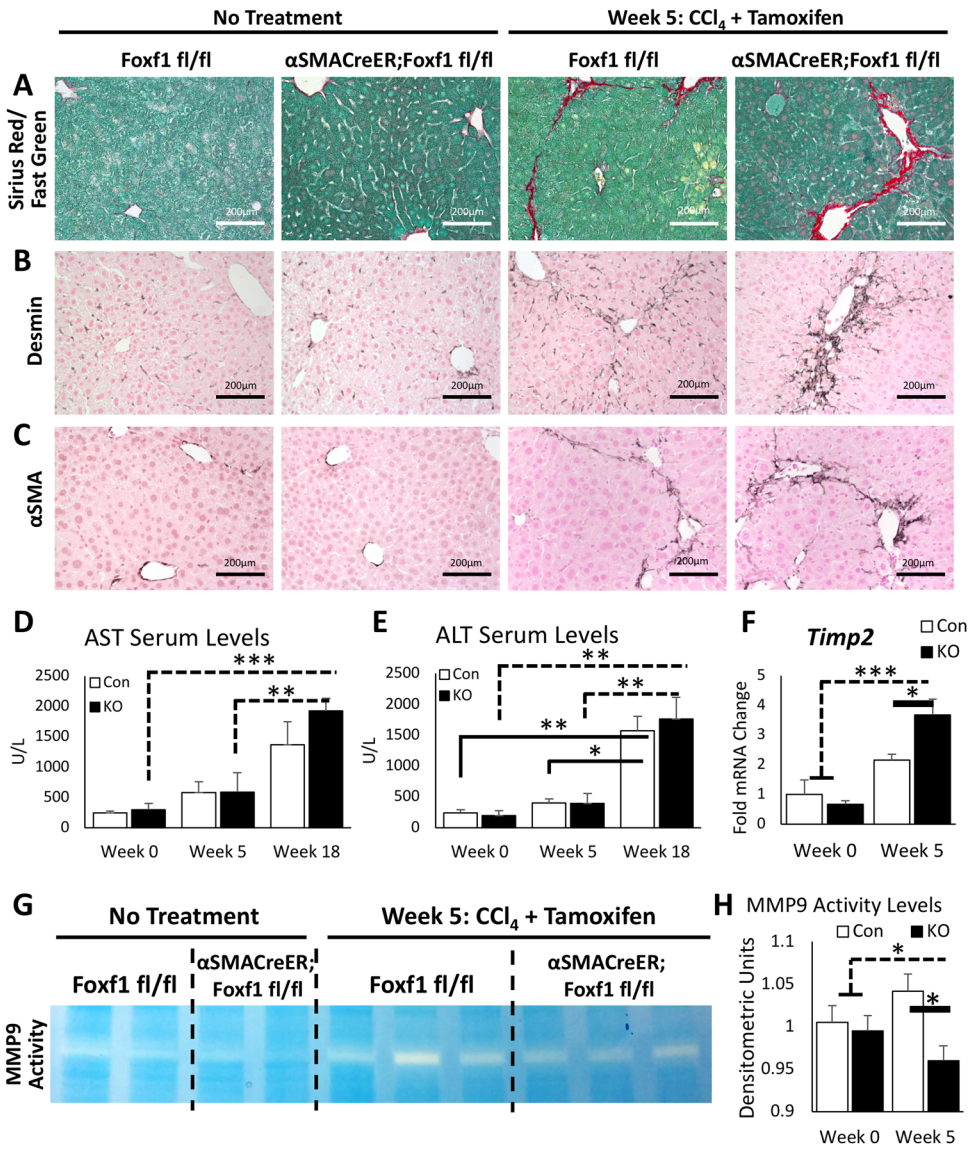

Fig. 3. Deletion of *Foxf1* from myofibroblasts increases liver fibrosis and inhibits MMP9 activity. (A) Sirius Red/Fast Green staining demonstrates increased collagen deposition between portal triads in CCl_4-treated *αSMACreER;Foxf1*$^{-/-}$ livers. (B,C) Immunohistochemistry shows increased staining for DES and αSMA in CCl_4-treated *αSMACreER;Foxf1*$^{-/-}$ livers. (D,E) Serum enzymatic analysis demonstrates increased AST and ALT levels after chronic CCl_4-induced liver injury. *Foxf1* deletion does not affect AST or ALT in blood serum. For AST levels: n=3 control mice and n=4 KO mice in week 0; n=5 control mice and n=5 KO mice in week 5; n=4 control mice and n=7 KO mice in week 18. For ALT levels: n=5 control mice and n=6 KO mice in week 0; n=7 control mice and n=8 KO mice in week 5; n=4 control mice and n=7 KO mice in week 18. (F) Increased *Timp2* mRNA in CCl_4-treated *αSMACreER;Foxf1*$^{-/-}$ livers is found by qRT-PCR. (G) Representative zymography gel shows decreased MMP9 activity in CCl_4-treated *αSMACreER;Foxf1*$^{-/-}$ livers. Cropped gel is presented here with full gel presented in Fig. S12. (H) Quantification of zymography gels reveals a significant decrease in MMP9 activity in CCl_4-treated *αSMACreER;Foxf1*$^{-/-}$ livers. Quantification was averaged across three gels. *P<0.05, **P<0.01, ***P<0.001.

CCl_4-treated livers by co-localization of Ki-67 with DES (Fig. 4E) and αSMA (Fig. S9); however, there were no changes in the number of Ki-67-positive HSCs and MFs after deletion of *Foxf1* (Fig. 4F). Protein levels of proliferation-specific genes FOXM1 and CCND1 were unaltered in *αSMACreER;Foxf1*$^{-/-}$ livers compared to controls (Fig. 4G). Thus, *Foxf1* deletion does not affect proliferation of HSCs and MFs after chronic CCl_4 liver injury.

RNA-seq analysis identified direct FOXF1 target genes critical for ECM deposition and hepatic fibrosis

In order to identify FOXF1 target genes, RNA-seq (GEO accession GSE123726) was performed on primary hepatic stromal cells (containing MFs and HSCs) isolated from CCl_4-treated *Foxf1*$^{fl/fl}$ and *αSMACreER;Foxf1*$^{-/-}$ livers. Purified cells expressed *Des* and *Acta2*, but lacked hepatocyte (Nikoozad et al., 2014) and Kupffer cell (Yang et al., 2013) markers (Fig. S10). *Foxf1* mRNA was lost in isolated *αSMACreER;Foxf1*$^{-/-}$ stromal cells (Fig. 5A), a finding consistent with efficient deletion of *Foxf1* from CCl_4-treated livers. The RNA-seq was used to compare differential gene expression patterns between the *Foxf1*$^{fl/fl}$ and *αSMACreER;Foxf1*$^{-/-}$ stromal cells. The differential gene expression in the two groups are represented in a heat map (Fig. 5B). Gene ontology demonstrated that increased functional pathways for the *αSMACreER;Foxf1*$^{-/-}$ mice were related to ECM regulation, while decreased functional pathways included normal liver functions and metabolism (Fig. 5C). RNA-seq analysis was cross referenced with FOXF1 ChIP-seq analysis (GEO accession GSE100149). 905 genes were common between RNA-seq and ChIP-seq (Fig. 5D), which include 74 genes related to ECM deposition and fibrosis. ChIP-seq proximity analysis revealed that 20 of these ECM genes had FOXF1 binding sites within 2KB of the transcription start site (Fig. 5E).

Interestingly, *Col1α2*, *Col5α2* and *Mmp2* were among the 20 ECM-related genes that had FOXF1 binding sites within the gene loci (Fig. S11, Table S1). COL1α2 and COL5α2 are common ECM components in fibrotic livers (Mak et al., 2016), whereas MMP2 is a collagenase that is increased during liver fibrosis and associated with disease progression (Benyon et al., 1996). Expression of *Col1α2*, *Col5α2* and *Mmp2* mRNAs were increased in CCl_4-treated *αSMACreER;Foxf1*$^{-/-}$ livers as shown by RNA-seq and qRT-PCR (Fig. 5E, Fig. 6D), suggesting a negative regulation by FOXF1. The presence of gene silencing histone methylation marks H3K9me3 and H3K27me3 (Dong and Weng, 2013; Bernstein et al., 2006) in

Biology Open (2019) 8, bio039800. doi:10.1242/bio.039800

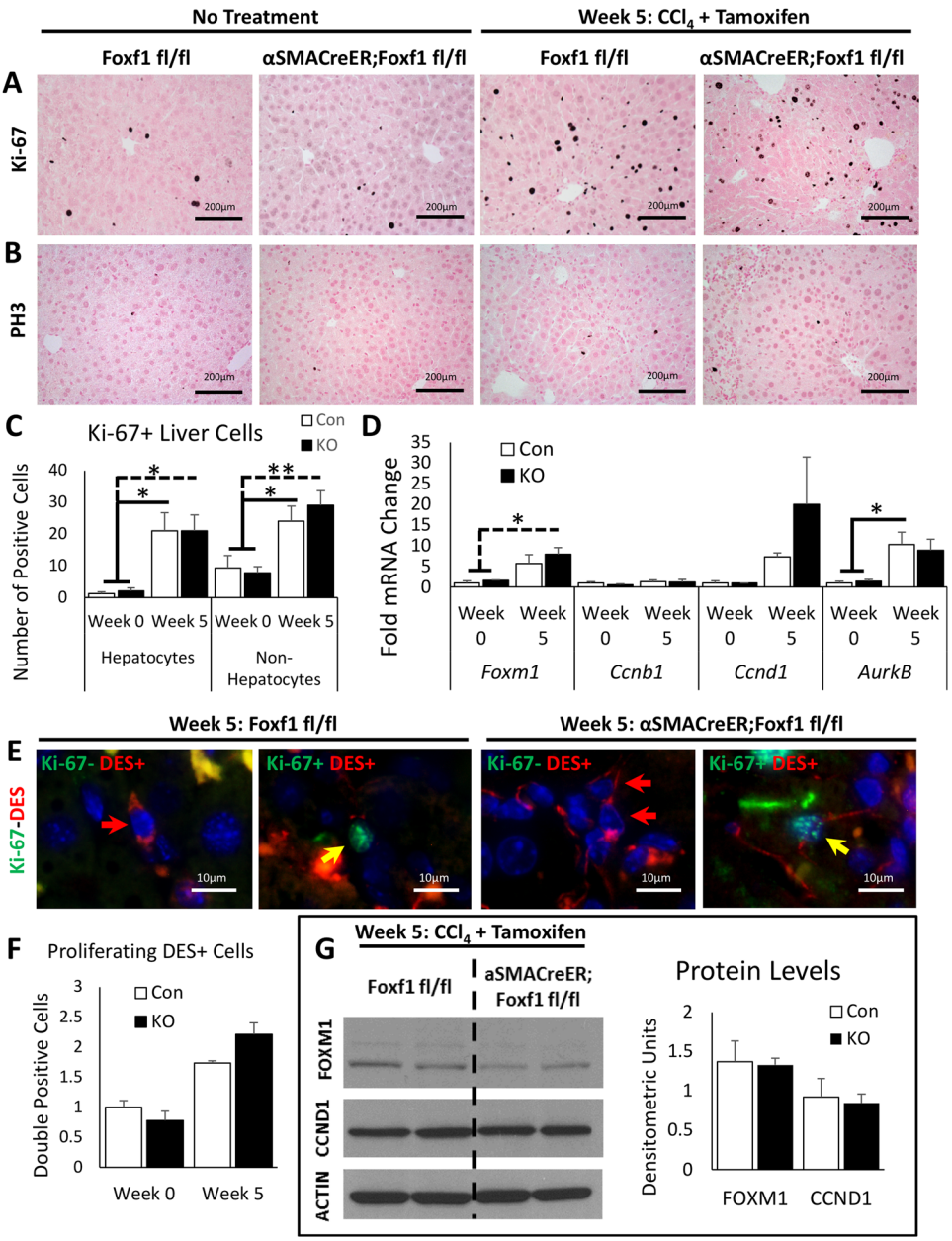

Fig. 4. Deletion of *Foxf1* does not influence proliferation of hepatic myofibroblasts. (A) Ki-67 staining shows a significant increase in cell proliferation following CCl_4-induced liver injury. No difference in Ki-67 staining is detected between $Foxf1^{fl/fl}$ and $\alpha SMACreER;Foxf1^{-/-}$ livers. (B) PH3 staining shows no significant changes in mitotic rates between $Foxf1^{fl/fl}$ and $\alpha SMACreER;Foxf1^{-/-}$ livers. (C) The number of Ki-67$^+$ hepatocytes and non-hepatocytes in $Foxf1^{fl/fl}$ livers was similar to those in $\alpha SMACreER;Foxf1^{-/-}$ livers. Numbers of Ki-67$^+$ cells were counted in 20–25 random 200× microscope fields using n=3 mice per group in week 0 and n=7 control mice and n=6 KO mice in week 5. (D) qRT-PCR was used to measure mRNAs in whole liver RNA. mRNAs were normalized to *Actb*. n=3 mice per group in week 0; n=5 mice per group in week 5. (E) Co-localization of Ki-67 with DES shows the presence of Ki-67$^+$ MFs in livers of CCl_4-treated mice. (F) Quantification of co-localization of Ki-67 with DES shows no difference in the number of Ki-67$^+$ DES$^+$ cells in $Foxf1^{fl/fl}$ livers compared to $\alpha SMACreER;Foxf1^{-/-}$ livers. (G) Western blot shows no significant difference in total liver protein levels of FOXM1 and CCND1 between $Foxf1^{fl/fl}$ and $\alpha SMACreER;Foxf1^{-/-}$ livers. Cropped blots are presented here with full length blots presented in Fig. S12. *P<0.05, **P<0.01.

FOXF1-binding promoter regions (Fig. 6A–C) is consistent with negative regulation of these genes by FOXF1. In order to confirm the regulation of *Col1α2*, *Col5α2* and *Mmp2* by FOXF1, we overexpressed FOXF1 in isolated murine HSCs (Fig. 6E). Lentiviral-mediated overexpression of FOXF1 decreased *Col1α2* and *Mmp2 in vitro* (Fig. 6F). Thus, FOXF1 negatively regulates expression of pro-fibrotic genes in MFs. Altogether, FOXF1 expression in myofibroblasts is essential to inhibit liver fibrosis after chronic liver injury (Fig. 6G).

DISCUSSION

Myofibroblast activation is a key mechanism in the development of hepatic fibrosis. However, transcriptional regulation of myofibroblasts during liver fibrogenesis remains poorly characterized. In the present study, we found that the deletion of *Foxf1* in MFs during chronic CCl_4-mediated injury exacerbated liver fibrosis, increased collagen deposition and stimulated expression of pro-fibrotic genes. ECM-related proteins were identified as novel FOXF1 transcriptional targets, suggesting that FOXF1 plays an important role in the regulation of ECM and collagen deposition during the progression of hepatic fibrosis.

Previous studies have focused on the role of FOXF1 in acute liver injury using a single CCl_4 administration to $Foxf1^{+/-}$ mice. These studies demonstrated that FOXF1 is necessary for HSC activation to promote liver repair (Kalinichenko et al., 2003). CCl_4-treated $Foxf1^{+/-}$ mice exhibited diminished collagen depositions and increased mortality after the liver injury (Kalinichenko et al., 2003). A recently published model of *Foxf1*-silencing using a lipid-based nanoparticle system to deliver *Foxf1* siRNA to the liver demonstrated attenuated collagen deposition when *Foxf1* siRNA was delivered 48 h prior to bile duct ligation (Abshagen et al., 2015). It is likely that *Foxf1* siRNA inhibited FOXF1 signaling in hepatic stellate cells, decreasing their activation and subsequent collagen depositions into the liver tissue, a finding consistent with previous studies using $Foxf1^{+/-}$ mice (Kalinichenko et al., 2003). Recently, a model of chronic hepatic injury using CCl_4-injections,

Biology Open (2019) 8, bio039800. doi:10.1242/bio.039800

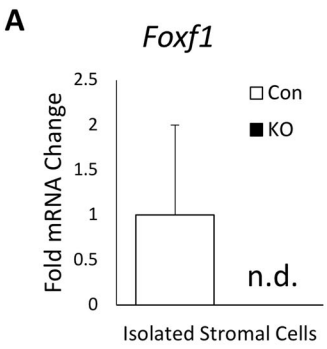

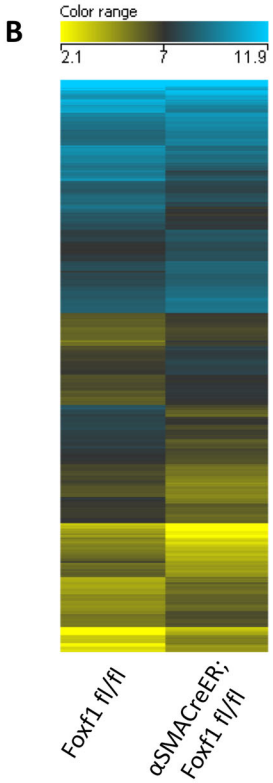

C

Gene Ontology: Increased Functional Pathways		
Functional Term	**P-Value**	**Genes**
Extracellular Matrix Organization	4.77E-12	39
Ensemble of Genes Encoding Core Extracellular Matrix	1.04E-09	36
Genes Encoding Collagen Proteins	1.56E-09	14
ECM-Receptor Interaction	1.90E-09	19
Integrin Signaling Pathway	6.25E-09	26

Gene Ontology: Decreased Functional Pathways		
Functional Term	**P-Value**	**Genes**
Metabolism	1.18E-43	190
Metabolism of Amino Acids and Derivatives	1.08E-21	46
Metabolism of Xenobiotics by Cytochrome P450	2.17E-18	27
Metabolism of Lipids and Lipoproteins	3.54E-17	74
Biological Oxidations	1.63E-15	35

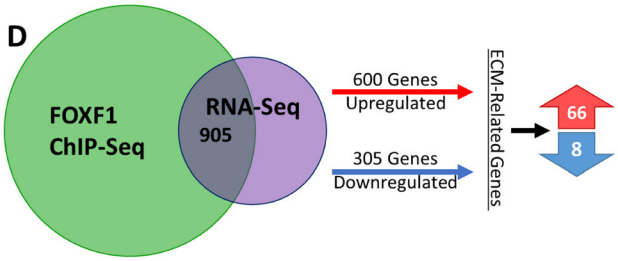

E

Genes Modified with FOXF1 Binding 2KB from Transcription Start Site			
Gene Symbol	**Entrez ID**	**Fold Change**	**P-value**
Fn1	14268	2.55	0
Lepr	16847	2.19	2.46E-06
Flrt2	399558	1.73	9.22E-07
Adamts14	237360	1.68	0.00464547
Fryl	72313	1.67	2.13E-14
Ssh2	237860	1.67	9.57E-16
Camsap1	227634	1.65	1.30E-05
Ahnak	66395	1.64	0
Exoc4	20336	1.62	1.09E-05
Nckap1	50884	1.61	4.76E-09
Clasp1	76707	1.57	1.69E-04
Mmp2	17390	1.56	0.0202771
Col4α5	12830	1.53	5.82E-04
Col1α2	12843	1.53	0
Col5α2	12832	1.51	4.07E-19
Vcl	22330	1.50	6.92E-15
Dctn3	53598	-1.64	3.25E-06
Pcolce2	76477	-1.84	0
Itih1	16424	-2.29	0
Fgl1	234199	-5.52	0

Fig. 5. FOXF1 deletion alters expression of pro-fibrotic genes in hepatic myofibroblasts. (A) qRT-PCR analysis of primary hepatic stromal cells submitted for RNA sequencing shows that *Foxf1* mRNA is not detected (n.d.) in *αSMACreER; Foxf1*$^{-/-}$ livers. Samples were pooled for further analysis. (B) Heat map shows differentially expressed genes in stromal cells from *Foxf1*$^{fl/fl}$ and *αSMACreER; Foxf1*$^{-/-}$ livers after chronic CCl_4-induced hepatic injury as identified by RNA-seq analysis. (C) Biological processes influenced by the deletion of *Foxf1* were identified using ToppFunn. *P*-values and number of genes are listed for each classification. (D) 905 overlapping genes were identified between ChIP-seq (GEO accession GSE100149) and RNA-seq (GEO accession GSE123726) data, of which 74 were ECM-related genes. (E) Table shows 20 ECM-related genes identified by ChIP-seq and RNA-seq (FOXF1 binding was analyzed within 2 KB from transcriptional start site).

similar to the present study, was unsuccessful in silencing *Foxf1* expression using the same lipid based system to deliver *Foxf1* siRNA (Abshagen et al., 2015, 2017). This method involved four weeks of IP CCl_4-injections before two weeks of treatment with *Foxf1* siRNA (Abshagen et al., 2017). It is possible that the lack of *Foxf1* silencing was due to inability of nanoparticles to target hepatic MFs. In the current study, we utilized a conditional genetic mouse model to delete *Foxf1* in MFs during CCl_4-induced hepatic fibrosis which shares multiple histological similarities with human disease (Masugi et al., 2018; Bataller and Brenner, 2005). Interestingly, the loss of *Foxf1* in MFs resulted in increased collagen deposition, causing severe fibrotic lesions between hepatic portal triads in *αSMACreER;Foxf1*$^{-/-}$ livers. Our studies suggest that FOXF1 inhibits production of collagen and ECM during the progression of liver fibrosis. Increased fibrosis in *Foxf1*-deficient mice was associated with the appearance of liver tumors, a finding consistent with increased tumor formation in patients with liver cirrhosis (EASL-EORTC et al., 2018). Our studies suggest that maintaining *Foxf1* expression can be beneficial in patients with advanced liver fibrosis to inhibit fibrotic responses and decrease the risk of liver tumorigenesis.

In the present study, collagens were significantly increased in *αSMACreER;Foxf1*$^{-/-}$ livers after chronic CCl_4-treatment. Desmin and αSMA were both increased in *αSMACreER;Foxf1*$^{-/-}$ livers; however, there were no differences in the number of proliferating cells between *Foxf1*$^{fl/fl}$ and *αSMACreER;Foxf1*$^{-/-}$ livers. Previously, FOXF1 has been shown to stimulate cell proliferation in lung endothelial cells (Ren et al., 2014; Bolte et al., 2017) and in rhabdomyosarcoma tumor cells (Milewski et al., 2017). Surprisingly, we found that deletion of *Foxf1* from MFs does not affect their proliferation during liver fibrogenesis. It is possible that FOXF1 requires additional co-activator or co-repressor proteins (that are not present in MFs) to regulate cellular proliferation. Additionally, we found an increase in *Timp2* expression with a decrease in MMP9 activity in *αSMACreER;Foxf1*$^{-/-}$ livers. Since it is well-known that TIMPs and MMPs regulate ECM depositions to

Biology Open (2019) 8, bio039800. doi:10.1242/bio.039800

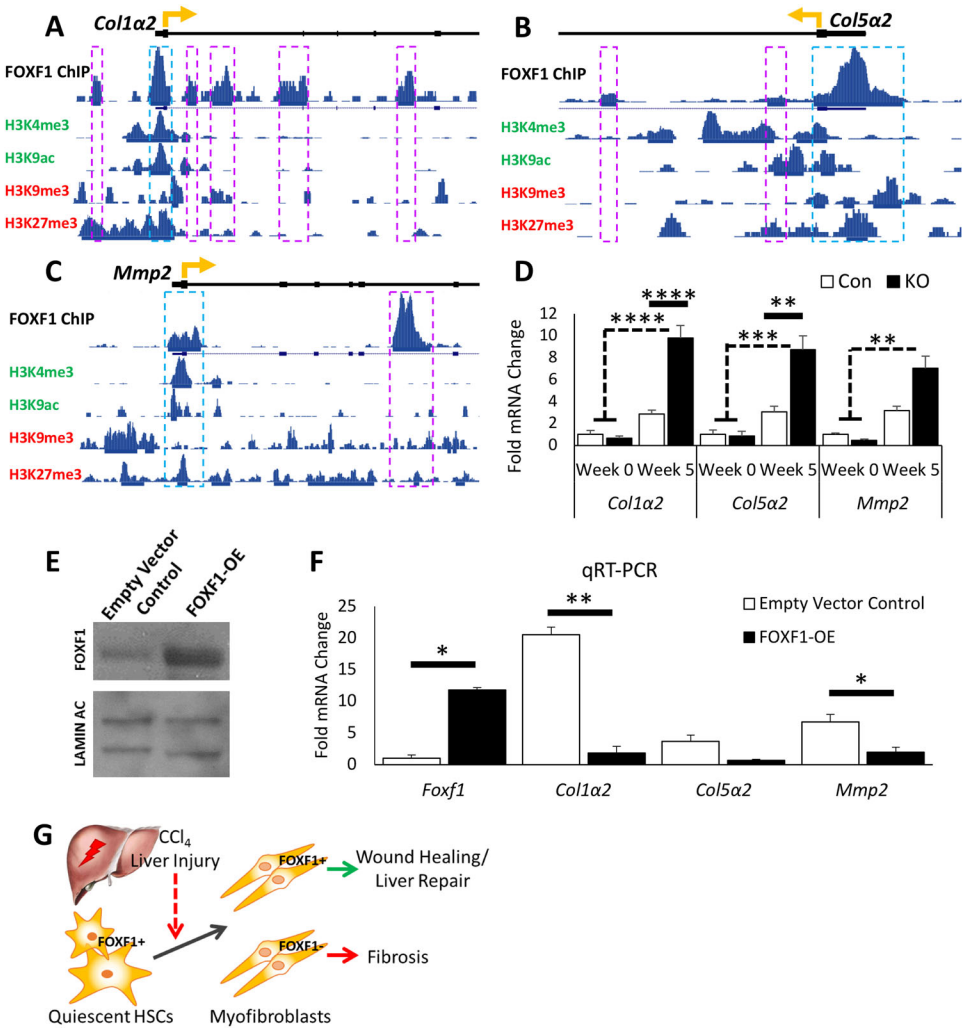

Fig. 6. FOXF1 binds to DNA regulatory regions of *Col1α2*, *Col5α2* and *Mmp2*. (A–C) ChIP-seq shows FOXF1 binding near the transcriptional start sites in *Col1α2*, *Col5α2* and *Mmp2* gene loci. Histone modification marks of enhancers (H3K4me3, H3K9ac) and repressors (H3K9me3, H3K27me3) are aligned with FOXF1-binding regions. Significant areas of FOXF1 binding are marked with boxes, with blue boxes indicating the binding site is within gene promoter region. Gene transcriptional start sites are marked with a directional yellow arrow. (D) qRT-PCR analysis shows the significant increase of *Col1α2*, *Col5α2* and *Mmp2* mRNAs in the isolated stromal cells of CCl_4-treated *αSMACreER;Foxf1*$^{-/-}$ livers. For *Col1α2* and *Col5α2*: *n*=3 mice per group in week 0; *n*=5 mice per group in week 5. For *Mmp2*: *n*=3 mice per group in week 0; *n*=6 control mice and *n*=4 KO mice in week 5. (E) Western blot shows increase in FOXF1 expression in isolated HSCs after FOXF1-overexpression. Cropped blots are presented here with full length blots presented in Fig. S12. (F) qRT-PCR shows an increase of *Foxf1* mRNA and a decrease of *Col1α2*, *Col5α2* and *Mmp2* mRNAs in isolated HSCs after FOXF1-overexpression. (G) Diagram of hepatic fibrosis in *Foxf1*-deficient mice shows that the loss of FOXF1 promotes ECM deposition and exacerbated fibrosis after CCl_4-treatment. **P*<0.05, ***P*<0.01, ****P*<0.001, *****P*<0.0001.

balance the scaring and healing processes during fibrosis (Duarte et al., 2015), it is possible that the loss of *Foxf1* alters the TIMP/MMP balance to allow accumulation of collagens without the degradation mechanisms necessary for proper wound healing. Interestingly, MMP9 has been implicated in HSC to MF transdifferentiation (Han et al., 2007) in addition to its roles in ECM degradation (Duarte et al., 2015; Kurzepa et al., 2014). Therefore, decreased MMP9 activity can contribute to increased liver fibrosis in *αSMACreER;Foxf1*$^{-/-}$ mice. Surprisingly, FOXF1 was increased in activated HSCs compared to quiescent HSCs. It is possible that FOXF1 is differentially regulated in HSCs compared to hepatic MFs, and that after liver injury, FOXF1 protects HSCs from differentiating into MFs through transcriptional repression of profibrotic genes.

Consistent with increased fibrosis in *Foxf1*-deficient livers, RNA-seq analysis revealed increased ECM-related functional pathways in a purified stromal cell population. Comparison with FOXF1 ChIP-seq data revealed 20 novel transcriptional targets of FOXF1, which include *Col1α2*, *Col5α2* and *Mmp2*, expression of which was increased in *Foxf1*-deficient cells.

COL1α2 is one of the most abundant ECM components in the liver along with COL1α1 and COL3α1 (Lai et al., 2011). COL5α2 is highly expressed with Collagens 1 and 3 and is important in regulating the assembly and structure of these collagens in the fibrotic matrix (Moriya et al., 2011). MMP2 acts as a collagenase, known to be activated during hepatic fibrosis (Benyon et al., 1996). In addition to increased mRNA levels of the genes in FOXF1-deficient cells, we found multiple FOXF1 binding sites within their gene promoter region and introns, suggesting direct transcriptional repression. This hypothesis is supported by the presence of H3K4me3 and H3K9ac, histone modifications associated with transcriptional repression (Dong and Weng, 2013; Rea et al., 2000), at FOXF1 binding sites. In summary, we have developed a novel genetic mouse model to study the role of FOXF1 in MFs during chronic liver injury. Using this model, we demonstrated that *Foxf1* expression in MFs is necessary to inhibit hepatic fibrosis and maintain the balance of collagen depositions, through transcriptional repression of pro-fibrotic genes.

MATERIALS AND METHODS

Mice

The *Foxf1*$^{fl/fl}$ mouse line was previously generated and bred into the C57Bl/6 mouse background (Ren et al., 2014; Cai et al., 2016). *Foxf1*$^{fl/fl}$ mice were bred with *αSMA-CreER* mice (Jackson Laboratory, 029925; Wendling et al., 2009) to generate *αSMACreER;Foxf1*$^{fl/fl}$ mice (Black et al., 2018). *αSMACreER;Foxf1*$^{fl/fl}$ mice were bred with *Foxf1*$^{fl/fl}$ mice and male pups were genotyped and used for all experiments at the age of 6–8 weeks. The following primers were used for genotyping: *αSMA-CreER* sense: 5′ TGCAACGAGTGATGAGGTTCGC 3′ and anti-sense: 5′ GATCCTGGCAATTTCGGCTATACG 3′; *αSMA-WT* sense 5′ GGTTTCTATTGCTACCAAGAGACAT 3′ and anti-sense: 5′ TGCACCAAACCCTGGACTAAGCAT 3′; *Foxf1*$^{fl/fl}$ sense: 5′ GCTTTGTCTCCAAGCGCTGC 3′

and anti-sense: 5′ TTCAGATCTGAGAGTGGCAGCTTC 3′. *Foxf1*$^{fl/fl}$ littermates were used as controls. To activate the conditional *Foxf1* knockout, tamoxifen (Tam) was given via intraperitoneal injection (40 mg/kg of body weight; Sigma-Aldrich) three days in a row at the beginning of each week starting at week 2 over the course of the chronic liver injury period. Hepatic injury was induced by intraperitoneal injections of carbon tetrachloride (CCl_4; 1 µl/g of body weight 20% v/v; Sigma-Aldrich; diluted in sunflower seed oil) three times a week every other day over the course of the chronic liver injury period. The levels of aminotransferases AST and ALT, proteins albumin and globulin, and direct and indirect bilirubin were determined by serological analysis of blood serum as previously described (Sun et al., 2017; Ren et al., 2010). All animal studies were approved by the Institutional Animal Care and Use Committee (IACUC) of Cincinnati Children's Research Foundation and the NIH IACUC Guidebook. All experiments were covered under our animal protocol (IACUC2016-0038). The Cincinnati Children's Research Foundation Institutional Animal Care and Use Committee is an AAALAC and NIH accredited institution (NIH Insurance #8310801).

Histology and immunohistochemistry

Paraffin-embedded liver sections were used for H&E staining, immunohistochemistry (IHC), or immunofluorescence (IF) as previously described (Ren et al., 2010; Kalinichenko et al., 2003; Wang et al., 2003). The following antibodies were used for immunostaining: FOXF1 (1:1000 IHC, 1:200 IF, R&D Systems), DES (1:500 IHC, 1:100 IF; Santa Cruz Technologies), αSMA (1:10,000 IHC, 1:5000 IF; Sigma-Aldrich), Ki-67 (1:1000 IHC, 1:200 IF; Thermo Fisher Scientific), Ki-67 (1:200 IF; BD Biosciences), and PH3 (1:10,000 IHC; Santa Cruz Technologies). Antibody-antigen complexes were detected using biotinylated secondary antibodies followed by avidin-biotin-horseradish peroxidase complex and 3,3′diaminobenzidine substrate (Vector Labs) as previously described (Kalinichenko et al., 2003; Ren et al., 2010; Wang et al., 2012). Sections were counterstained with Nuclear Fast Red (Vector Labs). For immunofluorescence imaging, secondary antibodies conjugated with Alexa Fluor 488 or Alexa Fluor 594 (Invitrogen/Molecular Probes) were used as described (Ustiyan et al., 2012; Wang et al., 2010). Cell nuclei were counterstained with DAPI (Vector Labs). Masson's Trichrome (BD Biosciences) and Sirius Red/Fast Green (Chondrex, Inc.) specialty stains were performed according to the manufacturer's protocols. Brightfield images were obtained using a Zeiss AxioImage.A2 microscope. Fluorescent images were obtained using a Zeiss AxioPlan 2 microscope.

qRT-PCR, western blot, and zymography

The caudate lobe of the liver was halved and used for RNA and protein studies. RNA was isolated using RNA Stat-60 (Tel-Test, Inc.) according to the manufacturer's protocol and was reverse transcribed using the High Capacity Reverse Transcription Kit (Applied Biosystems) according to the manufacturer's protocol. mRNAs of specific genes were measured by qRT-PCR using TaqMan probes (Applied Biosystems; Table S2) and the StepOnePlus Real-Time PCR system (Applied Biosystems) as described (Bolte et al., 2011, 2015, 2012; Wang et al., 2010). mRNAs were normalized to *Actb*. Protein extracts were isolated using cell lysis buffer as previously described (Pradhan et al., 2016) and used for either western blot analysis with Pierce ECL western blotting substrate (Thermo Fisher Scientific) or gel zymography (NOVEX) according to the manufacturer's protocols. The following antibodies were used for protein blots: FOXF1 (1:1000, R&D Systems) (Bolte et al., 2017; Black et al., 2018; Ren et al., 2014), ACTIN (1:2000; Santa Cruz Biotechnology) (Pradhan et al., 2016), FOXM1 (1:3000; Santa Cruz Biotechnology) (Pradhan et al., 2016; Bolte et al., 2011), CCND1 (1:1000; Cell Signaling Technology) (Milewski et al., 2017). Protein band intensities were determined by ImageJ software and were normalized to ACTIN.

Hepatic stellate cell isolation, transfection

Hepatic stellate cells were isolated from male C57Bl/6-WT mice (40–50 g), purified using Nycodenz gradient, and cultured as previously described (Pradhan et al., 2016; Dangi et al., 2012; Sumpter et al., 2012). Quiescent HSCs were harvested at day two after cell culture (Reinehr et al., 1998). After ten days in culture, activated MFs were harvested (Reinehr et al., 1998). The pMIEG3 bicistronic retroviral vector was used for FOXF1 protein overexpression as previously described (Pradhan et al., 2016). The cells were transfected as previously described (Singh et al., 2008). mRNAs in isolated MFs were normalized to *18 s* (Eukaryotic 18S rRNA Endogenous Control; Applied Biosciences). Protein in isolated MFs were normalized to LAMIN AC (1:10,000; Santa Cruz Biotechnology) (Pradhan et al., 2016).

RNA sequencing

RNA was isolated from HSC/MF population purified from CCl_4-treated *Foxf1*$^{fl/fl}$ and *αSMACreER;Foxf1*$^{-/-}$ livers using a differential plating method (Giassetti et al., 2016) that we modified. Briefly, liver cell suspension was plated on tissue culture dishes (Corning) and incubated for 2 h at 37°C. Supernatant and non-adherent cells were washed off and the adherent cell population was collected for experiments. Samples were pooled to generate the libraries using the TruSeq RNA library preparation kit and were sequenced on an Illumina HiSeq 2000 sequencer, generating approximately 10 M high quality single end reads (75 base-long reads). Alignment was performed using the Tophat/Cufflink pipeline (Trapnell et al., 2009, 2010). Finally, cuffmerge tool was used to generate Binary Alignment/Map files (BAM files) (Roberts et al., 2011). BAM files of RNA-seq data were analyzed using Avadis® NGS Version 1.3.0 software. Reads were filtered to remove: (1) duplicate reads, (2) non-primary-matched reads, and (3) reads with alignment scores <95. Quantification was performed on the filtered reads against the RefSeq annotation. Data normalization was performed with the DESeq package. The sequencing depth was estimated by the read count of the gene with the median read count ratio across all genes. The method was based on the negative binomial distribution, which allows for less restrictive variance parameter assumptions than does the Poisson distribution. The false discovery rate was calculated according to the Benjamini and Hochberg algorithm (Benjamini and Hochberg, 1995). Genes with expression altered by a factor of 1.5 and a false discovery rate of 0.05 in *Foxf1*$^{fl/fl}$ cells compared with *αSMACreER;Foxf1*$^{-/-}$ cells were selected for gene set enrichment analysis using ToppGene Suite. Hierarchical clustering was performed by Ward's method using Euclidean distance metric. RNA-seq data are available at GEO accession GSE123726. RNA-seq data were compared to previously published ChIP-seq data (GEO accession GSE100149) using a two-way Venn diagram.

Statistical analysis

Statistical significance differences in measured variables between control and experimental groups were assessed with a Student's *t*-test (two-tailed) or one-way analysis of variance (ANOVA) with Bonferroni post hoc test as appropriate. $P<0.05$ was considered to be significant, with $P<0.05$ indicated with *, $P<0.01$ indicated with **, $P<0.001$ indicated with ***, and $P<0.0001$ indicated with ****. Values for all measurements were expressed as mean±s.e. of mean.

Competing interests

The authors declare no competing or financial interests.

Author contributions

Conceptualization: H.M.F., V.V.K.; Methodology: H.M.F.; Software: H.M.F.; Validation: H.M.F., N.D., V.V.K.; Formal analysis: H.M.F., C.B., N.D., A.S., Y.Z., C.R.G., T.V.K., V.V.K.; Investigation: H.M.F., C.B., A.S., Y.Z., C.R.G.; Resources: H.M.F.; Data curation: H.M.F.; Writing - original draft: H.M.F., V.V.K.; Writing - review & editing: H.M.F., C.B., N.D., A.S., Y.Z., C.R.G., T.V.K., V.V.K.; Visualization: H.M.F., V.V.K.; Supervision: H.M.F., V.V.K.; Project administration: H.M.F., V.V.K.; Funding acquisition: T.V.K., V.V.K.

Funding

We would like to acknowledge the following funding sources: National Institutes of Health Grants [HL84151 (V.V.K.), HL123490 (V.V.K.), HL141174 (V.V.K.), and HL132849 (T.V.K.)].

Data availability

The RNA sequencing microarray data presented in this article has been uploaded to Gene Expression Omnibus (GEO) database at the National Center for Biotechnology Information (NCBI) and the accession number is GSE123726.

Supplementary information

Supplementary information available online at
http://bio.biologists.org/lookup/doi/10.1242/bio.039800.supplemental

References

Abshagen, K., Brensel, M., Genz, B., Roth, K., Thomas, M., Fehring, V., Schaeper, U. and Vollmar, B. (2015). Foxf1 siRNA delivery to hepatic stellate cells by DBTC lipoplex formulations ameliorates fibrosis in livers of bile duct ligated mice. *Curr. Gene Ther.* **15**, 215-227.

Abshagen, K., Rotberg, T., Genz, B. and Vollmar, B. (2017). No significant impact of Foxf1 siRNA treatment in acute and chronic CCl4 liver injury. *Exp. Biol. Med. (Maywood)* **242**, 1389-1397.

Bachem, M., Sell, K.-M., Melchior, R., Kropf, J., Eller, T. & Gressner, A. (1993). Tumor necrosis factor alpha (TNFα) and transforming growth factor β1 (TGFβ1) stimulate fibronectin synthesis and the transdifferentiation of fat-storing cells in the rat liver into myofibroblasts. *Virchows Arch. B Cell Pathol. Incl. Mol. Pathol.* **63**, 123-130.

Bataller, R. and Brenner, D. A. (2005). Liver fibrosis. *J. Clin. Invest.* **115**, 209-218.

Benjamini, Y. and Hochberg, Y. (1995). Controlling the false discovery rate-a practical and powerful approach to multiple testing. *J. R. Stat. Soc. Series B Methodol.* **57**, 289-300.

Benyon, R. C., Iredale, J. P., Goddard, S., Winwood, P. J. and Arthur, M. J. (1996). Expression of tissue inhibitor of metalloproteinases 1 and 2 is increased in fibrotic human liver. *Gastroenterology* **110**, 821-831.

Bernstein, B. E., Mikkelsen, T. S., Xie, X., Kamal, M., Huebert, D. J., Cuff, J., Fry, B., Meissner, A., Wernig, M., Plath, K. et al. (2006). A bivalent chromatin structure marks key developmental genes in embryonic stem cells. *Cell* **125**, 315-326.

Black, M., Milewski, D., Le, T., Ren, X., Xu, Y., Kalinichenko, V. V. and Kalin, T. V. (2018). FOXF1 inhibits pulmonary fibrosis by preventing CDH2-CDH11 cadherin switch in myofibroblasts. *Cell Rep* **23**, 442-458.

Bolte, C., Zhang, Y., Wang, I.-C., Kalin, T. V., Molkentin, J. D. and Kalinichenko, V. V. (2011). Expression of foxm1 transcription factor in cardiomyocytes is required for myocardial development. *PLoS ONE* **6**, e22217.

Bolte, C., Zhang, Y., York, A., Kalin, T. V., Schultz, J. E. J., Molkentin, J. D. and Kalinichenko, V. V. (2012). Postnatal ablation of foxm1 from cardiomyocytes causes late onset cardiac hypertrophy and fibrosis without exacerbating pressure overload-induced cardiac remodeling. *PLoS ONE* **7**, e48713.

Bolte, C., Ren, X., Tomley, T., Ustiyan, V., Pradhan, A., Hoggatt, A., Kalin, T. V., Herring, B. P. and Kalinichenko, V. V. (2015). Forkhead box F2 regulation of platelet-derived growth factor and myocardin/serum response factor signaling is essential for intestinal development. *J. Biol. Chem.* **290**, 7563-7575.

Bolte, C., Flood, H. M., Ren, X., Jagannathan, S., Barski, A., Kalin, T. V. and Kalinichenko, V. V. (2017). FOXF1 transcription factor promotes lung regeneration after partial pneumonectomy. *Sci. Rep.* **7**, 10690.

Bolte, C., Whitsett, J. A., Kalin, T. V. and Kalinichenko, V. V. (2018). Transcription factors regulating embryonic development of pulmonary vasculature. *Adv. Anat. Embryol. Cell Biol.* **228**, 1-20.

Brenner, D. A., Kisseleva, T., Scholten, D., Paik, Y. H., Iwaisako, K., Inokuchi, S., Schnabl, B., Seki, E., De Minicis, S., Oesterreicher, C. et al. (2012). Origin of myofibroblasts in liver fibrosis. *Fibrogenesis Tissue Repair* **5**, S17-S17.

Cai, Y., Bolte, C., Le, T., Goda, C., Xu, Y., Kalin, T. V. and Kalinichenko, V. V. (2016). FOXF1 maintains endothelial barrier function and prevents edema after lung injury. *Sci. Signal.* **9**, ra40-ra40.

Cheng, K. and Mahato, R. I. (2007). Gene modulation for treating liver fibrosis. *Crit. Rev. Ther. Drug Carrier Syst.* **24**, 93-146.

Civan, J. (2016). *Hepatic and Biliary Diseases: Hepatic Fibrosis. Merck Manual: Professional Version*. Kenilworth, NJ, USA: Merck & Co., Inc.

Croci, I., Byrne, N. M., Choquette, S., Hills, A. P., Chachay, V. S., Clouston, A. D., O'moore-Sullivan, T. M., Macdonald, G. A., Prins, J. B. and Hickman, I. J. (2013). Whole-body substrate metabolism is associated with disease severity in patients with non-alcoholic fatty liver disease. *Gut* **62**, 1625-1633.

Dangi, A., Sumpter, T. L., Kimura, S., Stolz, D. B., Murase, N., Raimondi, G., Vodovotz, Y., Huang, C., Thomson, A. W. and Gandhi, C. R. (2012). Selective expansion of allogeneic regulatory T cells by hepatic stellate cells: role of endotoxin and implications for allograft tolerance. *J. Immunol.* **188**, 3667-3677.

Dong, X. and Weng, Z. (2013). The correlation between histone modifications and gene expression. *Epigenomics* **5**, 113-116.

Duarte, S., Baber, J., Fujii, T. and Coito, A. J. (2015). Matrix metalloproteinases in liver injury, repair and fibrosis. *Matrix Biol.* **44**, 147-156.

EASL-EORTC, LIVER, E. A. F. S. O. T. & CANCER, E. O. F. R. A. T. O. (2018). EASL clinical practice guidelines: management of hepatocellular carcinoma. *J. Hepatol.* **69**, 182-236.

Fausther, M., Lavoie, E. G. and Dranoff, J. A. (2013). Contribution of myofibroblasts of different origins to liver fibrosis. *Curr. Pathobiol. Rep.* **1**, 225-230.

Giassetti, M. I., Goissis, M. D., De Barros, F. R. O., Bruno, A. H., Assumpção, M. E. O. and Visintin, J. A. (2016). Comparison of diverse differential plating methods to enrich bovine spermatogonial cells. *Reprod. Domest. Anim.* **51**, 26-32.

Han, Y.-P., Yan, C., Zhou, L., Qin, L. and Tsukamoto, H. (2007). A matrix metalloproteinase-9 activation cascade by hepatic stellate cells in trans-differentiation in the three-dimensional extracellular matrix. *J. Biol. Chem.* **282**, 12928-12939.

Hellerbrand, C., Stefanovic, B., Giordano, F., Burchardt, E. R. and Brenner, D. A. (1999). The role of TGFβ1 in initiating hepatic stellate cell activation in vivo. *J. Hepatol.* **30**, 77-87.

Hodo, Y., Honda, M., Tanaka, A., Nomura, Y., Arai, K., Yamashita, T., Sakai, Y., Yamashita, T., Mizukoshi, E., Sakai, A. et al. (2013). Association of interleukin-28B genotype and hepatocellular carcinoma recurrence in patients with chronic hepatitis C. *Clin. Cancer Res.* **19**, 1827-1837.

Kalin, T. V., Ustiyan, V. and Kalinichenko, V. V. (2011). Multiple faces of FoxM1 transcription factor: lessons from transgenic mouse models. *Cell Cycle* **10**, 396-405.

Kalinichenko, V. V., Zhou, Y., Shin, B., Stolz, D. B., Watkins, S. C., Whitsett, J. A. and Costa, R. H. (2002). Wild-type levels of the mouse Forkhead Box f1 gene are essential for lung repair. *Am. J. Physiol. Lung Cell. Mol. Physiol.* **282**, L1253-L1265.

Kalinichenko, V. V., Bhattacharyya, D., Zhou, Y., Gusarova, G. A., Kim, W., Shin, B. and Costa, R. H. (2003). Foxf1 +/– mice exhibit defective stellate cell activation and abnormal liver regeneration following CCl4 injury. *Hepatology* **37**, 107-117.

Kim, I.-M., Zhou, Y., Ramakrishna, S., Hughes, D. E., Solway, J., Costa, R. H. and Kalinichenko, V. V. (2005). Functional characterization of evolutionarily conserved DNA regions in forkhead box f1 gene locus. *J. Biol. Chem.* **280**, 37908-37916.

Kinnman, N., Goria, O., Wendum, D., Gendron, M. C., Rey, C., Poupon, R. and Housset, C. (2001). Hepatic stellate cell proliferation is an early platelet-derived growth factor-mediated cellular event in rat cholestatic liver injury. *Lab Invest.* **81**, 1709-1716.

Kurzepa, J., Madro, A., Czechowska, G., Kurzepa, J., Celiński, K., Kazmierak, W. and Slomka, M. (2014). Role of MMP-2 and MMP-9 and their natural inhibitors in liver fibrosis, chronic pancreatitis and non-specific inflammatory bowel diseases. *Hepatobiliary Pancreat. Dis. Int.* **13**, 570-579.

Lai, K. K. Y., Shang, S., Lohia, N., Booth, G. C., Masse, D. J., Fausto, N., Campbell, J. S. and Beretta, L. (2011). Extracellular matrix dynamics in hepatocarcinogenesis: a comparative proteomics study of PDGFC transgenic and pten null mouse models. *PLoS Genet.* **7**, e1002147.

Mahlapuu, M., Ormestad, M., Enerback, S. and Carlsson, P. (2001). The forkhead transcription factor Foxf1 is required for differentiation of extra-embryonic and lateral plate mesoderm. *Development* **128**, 155-166.

Mak, K. M., Png, C. Y. M. and Lee, D. J. (2016). Type V collagen in health, disease, and fibrosis. *Anat. Rec.* **299**, 613-629.

Makarev, E., Izumchenko, E., Aihara, F., Wysocki, P. T., Zhu, Q., Buzdin, A., Sidransky, D., Zhavoronkov, A. and Atala, A. (2016). Common pathway signature in lung and liver fibrosis. *Cell Cycle* **15**, 1667-1673.

Malarkey, D. E., Johnson, K., Ryan, L., Boorman, G. and Maronpot, R. R. (2005). New insights into functional aspects of liver morphology. *Toxicol. Pathol.* **33**, 27-34.

Martinez, A. K., Maroni, L., Marzioni, M., Ahmed, S. T., Milad, M., Ray, D., Alpini, G. and Glaser, S. S. (2014). Mouse models of liver fibrosis mimic human liver fibrosis of different etiologies. *Curr. Pathobiol. Rep.* **2**, 143-153.

Masugi, Y., Abe, T., Tsujikawa, H., Effendi, K., Hashiguchi, A., Abe, M., Imai, Y., Hino, K., Hige, S., Kawanaka, M. et al. (2018). Quantitative assessment of liver fibrosis reveals a nonlinear association with fibrosis stage in nonalcoholic fatty liver disease. *Hepatol. Commun.* **2**, 58-68.

Mederacke, I., Hsu, C. C., Troeger, J. S., Huebener, P., Mu, X., Dapito, D. H., Pradere, J.-P. and Schwabe, R. F. (2013). Fate-tracing reveals hepatic stellate cells as dominant contributors to liver fibrosis independent of its etiology. *Nat. Commun.* **4**, 2823-2823.

Milewski, D., Pradhan, A., Wang, X., Cai, Y., Le, T., Turpin, B., Kalinichenko, V. V. and Kalin, T. V. (2017). FoxF1 and FoxF2 transcription factors synergistically promote Rhabdomyosarcoma carcinogenesis by repressing transcription of p21(Cip1) CDK inhibitor. *Oncogene* **36**, 850-862.

Moriya, K., Bae, E., Honda, K., Sakai, K., Sakaguchi, T., Tsujimoto, I., Kamisoyama, H., Keene, D. R., Sasaki, T. and Sakai, T. (2011). A fibronectin-independent mechanism of collagen fibrillogenesis in adult liver remodeling. *Gastroenterology* **140**, 1653-1663.

Nikoozad, Z., Ghorbanian, M. T. and Rezaei, A. (2014). Comparison of the liver function and hepatic specific genes expression in cultured mesenchymal stem cells and hepatocytes. *Iran. J. Basic Med. Sci.* **17**, 27-33.

Pradhan, A., Ustiyan, V., Zhang, Y., Kalin, T. V. and Kalinichenko, V. V. (2016). Forkhead transcription factor FoxF1 interacts with Fanconi anemia protein complexes to promote DNA damage response. *Oncotarget* **7**, 1912-1926.

Rea, S., Eisenhaber, F., O'carroll, D., Strahl, B. D., Sun, Z.-W., Schmid, M., Opravil, S., Mechtler, K., Ponting, C. P., Allis, C. D. et al. (2000). Regulation of chromatin structure by site-specific histone H3 methyltransferases. *Nature* **406**, 593-599.

Reinehr, R. M., Kubitz, R., Peters-Regehr, T., Bode, J. G. and Häussinger, D. (1998). Activation of rat hepatic stellate cells in culture is associated with increased sensitivity to endothelin 1. *Hepatology* **28**, 1566-1577.

Ren, X., Zhang, Y., Snyder, J., Cross, E. R., Shah, T. A., Kalin, T. V. and Kalinichenko, V. V. (2010). Forkhead box M1 transcription factor is required for macrophage recruitment during liver repair. *Mol. Cell. Biol.* **30**, 5381-5393.

Ren, X., Shah, T. A., Ustiyan, V., Zhang, Y., Shinn, J., Chen, G., Whitsett, J. A., Kalin, T. V. and Kalinichenko, V. V. (2013). FOXM1 promotes allergen-induced goblet cell metaplasia and pulmonary inflammation. *Mol. Cell. Biol.* **33**, 371-386.

Ren, X., Ustiyan, V., Pradhan, A., Cai, Y., Havrilak, J. A., Bolte, C. S., Shannon, J. M., Kalin, T. V. and Kalinichenko, V. V. (2014). FOXF1 transcription factor is required for formation of embryonic vasculature by regulating VEGF signaling in endothelial cells. *Circ. Res.* **115**, 709-720.

Roberts, A., Pimentel, H., Trapnell, C. and Pachter, L. (2011). Identification of novel transcripts in annotated genomes using RNA-Seq. *Bioinformatics* **27**, 2325-2329.

Rockey, D. C., Weymouth, N. and Shi, Z. (2013). Smooth muscle α Actin (Acta2) and myofibroblast function during hepatic wound healing. *PLoS ONE* **8**, e77166.

Singh, T. R., Ali, A. M., Busygina, V., Raynard, S., Fan, Q., Du, C.-H., Andreassen, P. R., Sung, P. and Meetei, A. R. (2008). BLAP18/RMI2, a novel OB-fold-containing protein, is an essential component of the Bloom helicase-double Holliday junction dissolvasome. *Genes Dev.* **22**, 2856-2868.

Sumpter, T. L., Dangi, A., Matta, B. M., Huang, C., Stolz, D. B., Vodovotz, Y., Thomson, A. W. and Gandhi, C. R. (2012). Hepatic stellate cells undermine the allostimulatory function of liver myeloid dendritic cells via STAT3-dependent induction of IDO. *J. Immunol.* **189**, 3848-3858.

Sun, L., Ren, X., Wang, I.-C., Pradhan, A., Zhang, Y., Flood, H. M., Han, B., Whitsett, J. A., Kalin, T. V. and Kalinichenko, V. V. (2017). The FOXM1 inhibitor RCM-1 suppresses goblet cell metaplasia and prevents IL-13 and STAT6 signaling in allergen-exposed mice. *Sci. Signal.* **10**, eaai8583.

Trapnell, C., Pachter, L. and Salzberg, S. L. (2009). TopHat: discovering splice junctions with RNA-Seq. *Bioinformatics* **25**, 1105-1111.

Trapnell, C., Williams, B. A., Pertea, G., Mortazavi, A., Kwan, G., Van Baren, M. J., Salzberg, S. L., Wold, B. J. and Pachter, L. (2010). Transcript assembly and quantification by RNA-Seq reveals unannotated transcripts and isoform switching during cell differentiation. *Nat. Biotechnol.* **28**, 511-515.

Ustiyan, V., Wert, S. E., Ikegami, M., Wang, I.-C., Kalin, T. V., Whitsett, J. A. and Kalinichenko, V. V. (2012). Foxm1 transcription factor is critical for proliferation and differentiation of Clara cells during development of conducting airways. *Dev. Biol.* **370**, 198-212.

Wang, X., Bhattacharyya, D., Dennewitz, M. B., Kalinichenko, V. V., Zhou, Y., Lepe, R. and Costa, R. H. (2003). Rapid hepatocyte nuclear translocation of the Forkhead Box M1B (FoxM1B) transcription factor caused a transient increase in size of regenerating transgenic hepatocytes. *Gene Expr.* **11**, 149-162.

Wang, I.-C., Meliton, L., Ren, X., Zhang, Y., Balli, D., Snyder, J., Whitsett, J. A., Kalinichenko, V. V. and Kalin, T. V. (2009). Deletion of Forkhead Box M1 transcription factor from respiratory epithelial cells inhibits pulmonary tumorigenesis. *PLoS ONE* **4**, e6609.

Wang, I.-C., Zhang, Y., Snyder, J., Sutherland, M. J., Burhans, M. S., Shannon, J. M., Park, H. J., Whitsett, J. A. and Kalinichenko, V. V. (2010). Increased expression of FoxM1 transcription factor in respiratory epithelium inhibits lung sacculation and causes clara cell hyperplasia. *Dev. Biol.* **347**, 301-314.

Wang, I.-C., Snyder, J., Zhang, Y., Lander, J., Nakafuku, Y., Lin, J., Chen, G., Kalin, T. V., Whitsett, J. A. and Kalinichenko, V. V. (2012). Foxm1 mediates cross talk between kras/mitogen-activated protein kinase and canonical Wnt pathways during development of respiratory epithelium. *Mol. Cell. Biol.* **32**, 3838-3850.

Wendling, O., Bornert, J.-M., Chambon, P. and Metzger, D. (2009). Efficient temporally-controlled targeted mutagenesis in smooth muscle cells of the adult mouse. *Genesis* **47**, 14-18.

Wong, L., Yamasaki, G., Johnson, R. J. and Friedman, S. L. (1994). Induction of beta-platelet-derived growth factor receptor in rat hepatic lipocytes during cellular activation in vivo and in culture. *J. Clin. Investig.* **94**, 1563-1569.

Yang, C.-Y., Chen, J.-B., Tsai, T.-F., Tsai, Y.-C., Tsai, C.-Y., Liang, P.-H., Hsu, T.-L., Wu, C.-Y., Netea, M.-G., Wong, C.-H. and et al. (2013). CLEC4F is an inducible C-type lectin in F4/80-positive cells and is involved in alpha-galactosylceramide presentation in liver. *PLoS ONE* **8**, e65070.

Yin, C., Evason, K. J., Asahina, K. and Stainier, D. Y. R. (2013). Hepatic stellate cells in liver development, regeneration, and cancer. *J. Clin. Invest.* **123**, 1902-1910.

Yokoi, Y., Namihisa, T., Kuroda, H., Komatsu, I., Miyazaki, A., Watanabe, S. and Usui, K. (1984). Immunocytochemical detection of desmin in fat-storing cells (Ito Cells). *Hepatology* **4**, 709-714.

Gene	Chromosome	TSS	FOXF1 Binding Site	
Col1a2	6	4,505,910	-1331	-1182
			-294	57
			368	524
			810	1167
			2017	2499
			4134	4416
			22703	22845
			31422	31862
			32255	32529
			32776	31022
Col5a2	1	45,502,820	-816	33
			304	472
			1904	2052
			7190	7332
			9270	9637
			10489	10681
			12506	12937
			14086	14369
			55083	55225
			82266	82514
			122097	122457
Mmp2	8	92,827,778	-573	439
			6349	7508
			19004	20139
			21290	21848

Table S1. FOXF1 binding sites as identified by ChIP-seq relative to the transcriptional start site.

Gene Name	Assay Number
Actb	Mm00607939_s1
Acta2	Mm00725412_s1
Alb	Mm00802090_m1
AurkB	Mm01718146_g1
Cdkn1a	Mm01303209_m1
Cdkn1b	Mm00438168_m1
Ccnb1	Mm00838401_m1
Ccnd1	Mm00432359_m1
Clec4f	Mm00443934_m1
Col1a1	Mm00801666_g1
Col1a2	Mm00483888_m1
Col3a1	Mm00802331_m1
Col5a2	Mm00483675_m1
Des	Mm00802455_m1
Foxf1	Mm00487497_m1
Foxm1	Mm00514924_m1
Mmp13	Mm00624354_m1
Mmp16	Mm01210646_m1
Mmp2	Mm00439498_m1
Mmp8	Mm00439509_m1
Mmp9	Mm00442991_m1
Timp1	Mm00441818_m1
Timp2	Mm00441825_m1
Timp3	Mm00441826_m1

Table S2. List of TaqMan probes used in qRT-PCR analysis.

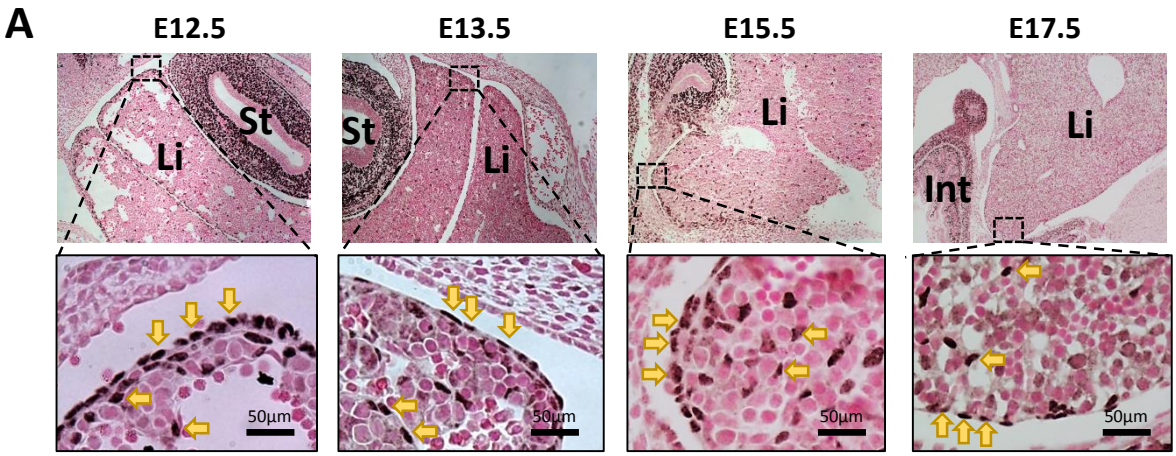

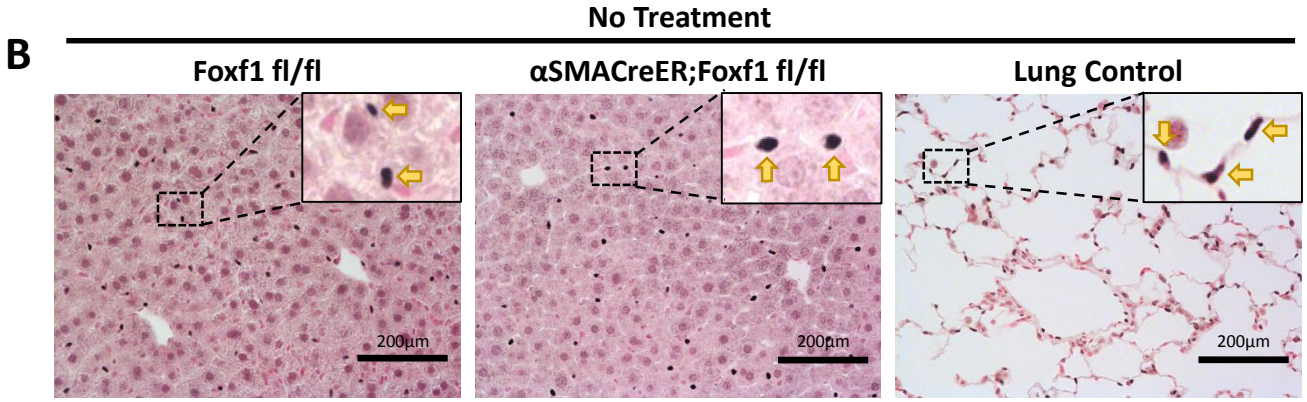

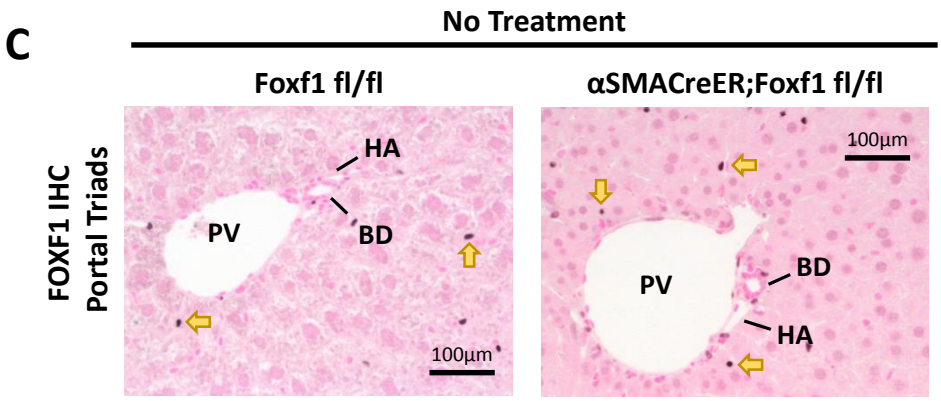

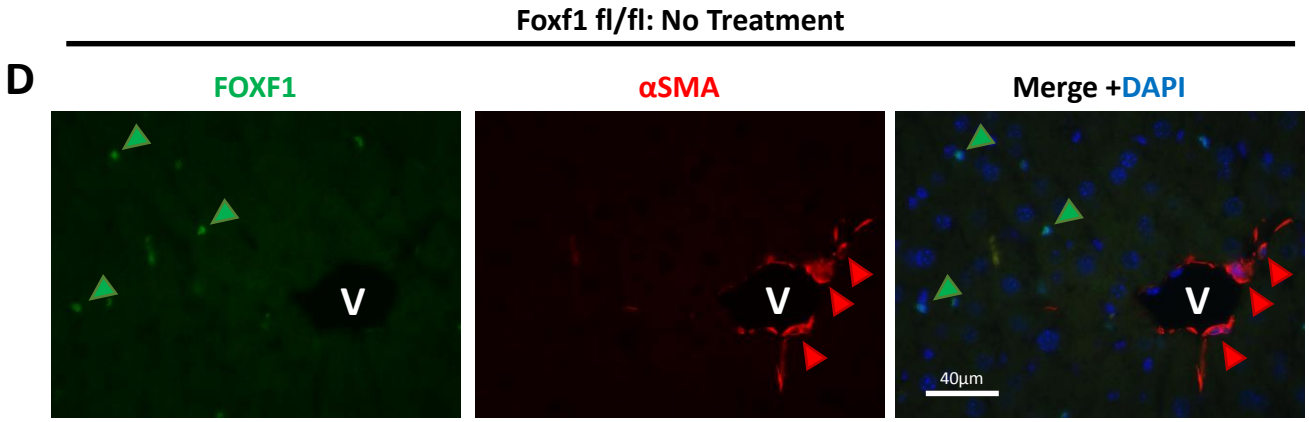

Figure S1. FOXF1 expression in mouse livers. (A) Immunostaining shows FOXF1 protein (dark brown) in nuclei of mesenchymal cells surrounding stomach (st) and intestine (int) of e12.5-17.5 mouse embryos. FOXF1 (yellow arrow) is also detected in mesothelial and stellate cells of the liver (li). Slides were counterstained with nuclear fast red (red). (B) Immunostaining shows FOXF1 (yellow arrow) expression in HSCs of uninjured livers. Lung sections were used as positive control for FOXF1 staining. (C) Immunostaining shows that FOXF1 (yellow arrow) is expressed in liver parenchyme but not in endothelial cells lining the portal vein (PV) and hepatic artery (HA). Bile ducts are shown as BD. (D) Co-localization of FOXF1 (green arrowheads) with αSMA (red arrowheads) shows that FOXF1 is not expressed in smooth muscle cells surrounding the portal vein (V) in uninjured *Foxf1*$^{fl/fl}$ livers.

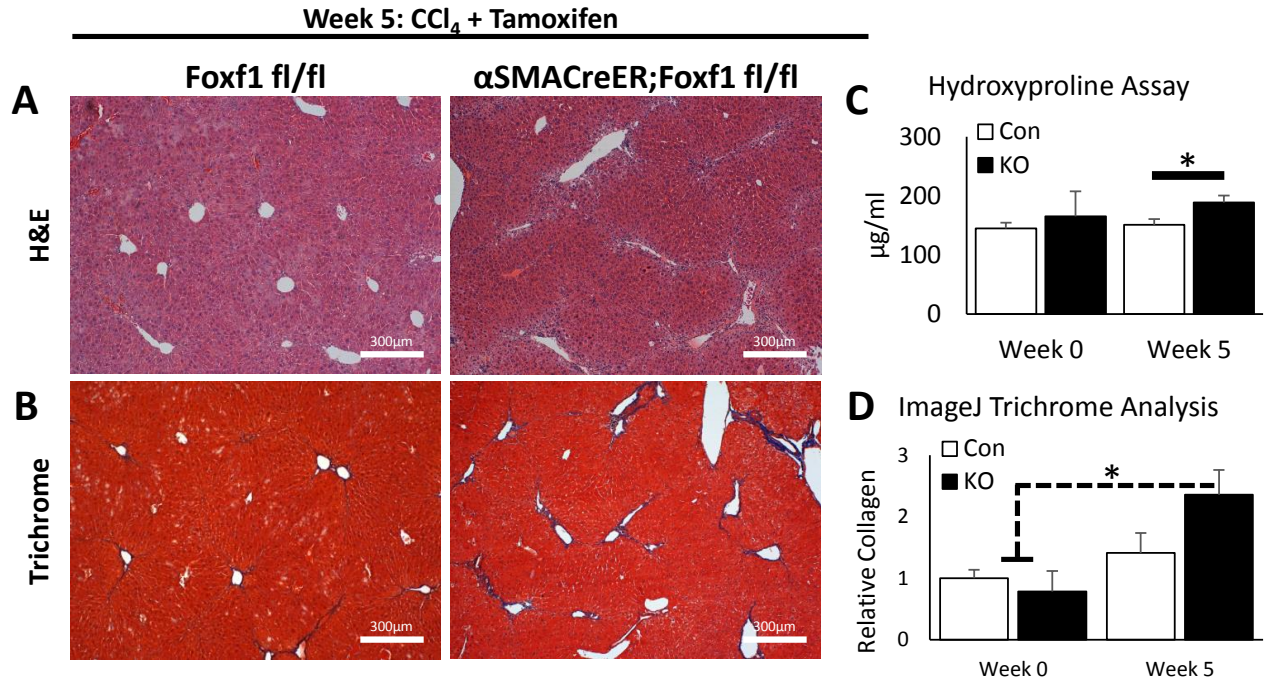

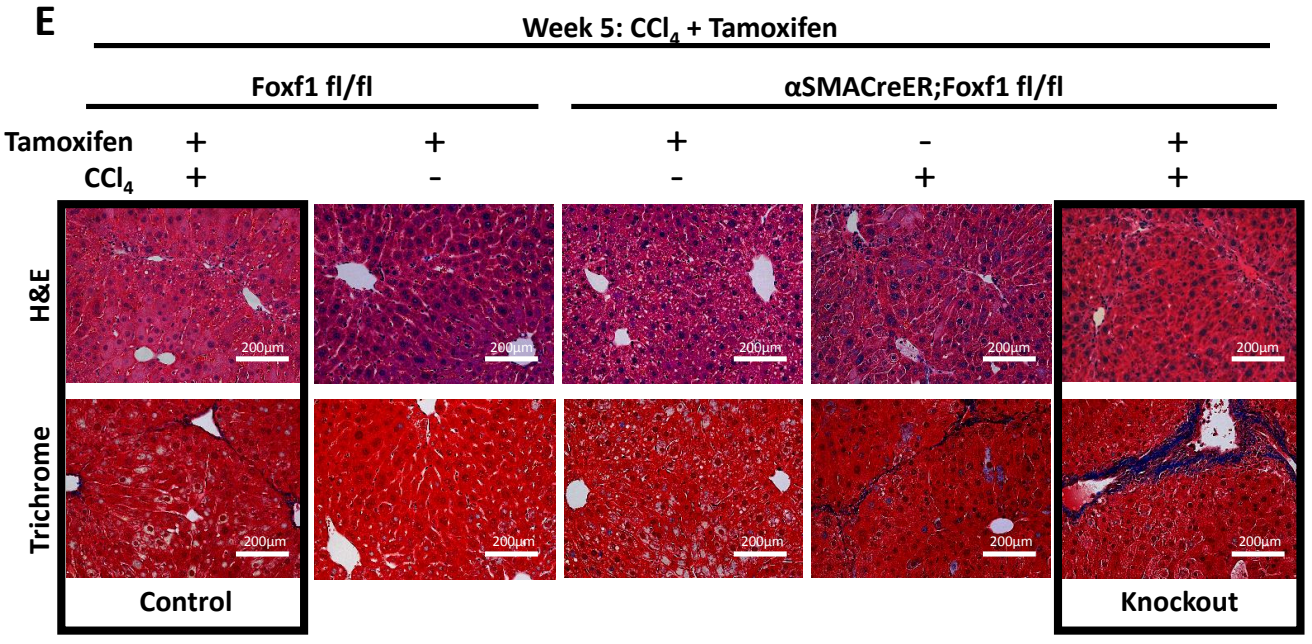

Figure S2. Treatment with tamoxifen alone does not induce hepatic fibrosis. (A) H&E and (B) Masson's trichrome staining of *Foxf1*$^{fl/fl}$ and *αSMACreER;Foxf1*$^{fl/fl}$ livers after 5-weeks of CCl_4 and Tam treatment show widespread hepatic fibrosis. (C) Collagen deposition was quantitated using the Hydroxyproline assay. n=2 mice per group in week 0; n=4 mice per group in week 5. (D) ImageJ analysis of Masson's trichrome images shows a significant increase in collagen in livers from *αSMACreER;Foxf1*$^{-/-}$ mice. n=3 mice per group in week 0; n=5 mice per group in week 5. (E) H&E and Masson's trichrome staining of *Foxf1*$^{fl/fl}$ and *αSMACreER;Foxf1*$^{fl/fl}$ livers from mice treated with Tam alone or in combination with CCl_4. Tam treatment does not induce hepatic fibrosis in either *Foxf1*$^{fl/fl}$ or *αSMACreER;Foxf1*$^{fl/fl}$ mice. Tam-mediated deletion of *Foxf1* exacerbates the fibrotic phenotype observed in CCl_4-treated *αSMACreER;Foxf1*$^{-/-}$ livers. P<0.05 is indicated with *.

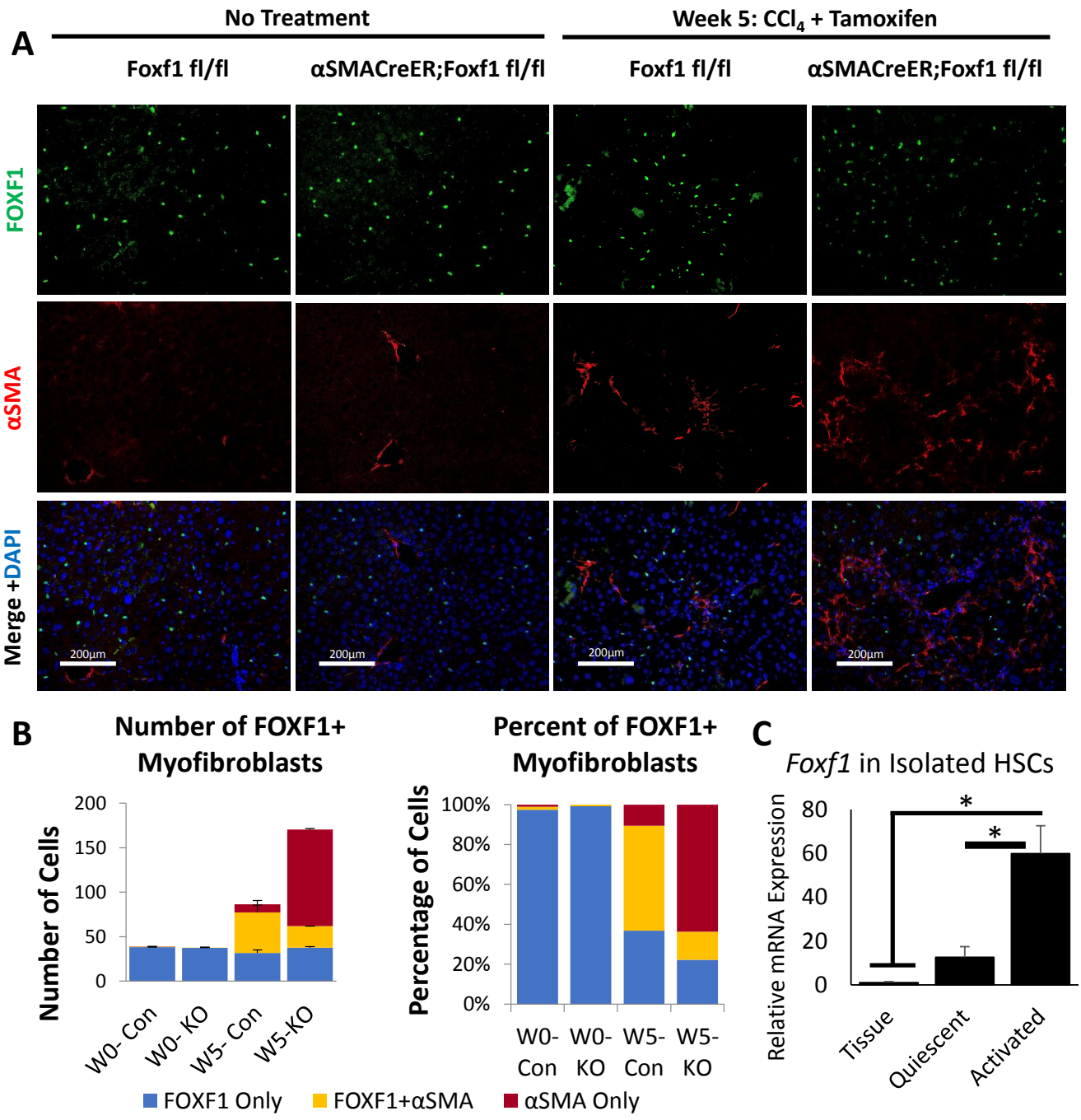

Figure S3. Number and percentage of FOXF1+ myofibroblasts are reduced in αSMACreER;Foxf1$^{-/-}$ livers. (A) Co-localization of FOXF1 with αSMA in *Foxf1*$^{fl/fl}$ and *αSMACreER;Foxf1*$^{-/-}$ livers. Scale bars 200 μm. (B) Counts of cells double stained for FOXF1 and αSMA show an increased number and percentage of αSMA+ FOXF1- MFs in CCl_4-treated *αSMACreER;Foxf1*$^{-/-}$ livers compared to controls (W0 is Week 0; W5 is Week 5). (C) qRT-PCR shows a significant increase in *Foxf1* mRNA in HSCs isolated from C57Bl/6-WT mice at the activated stage compared to uninjured livers.

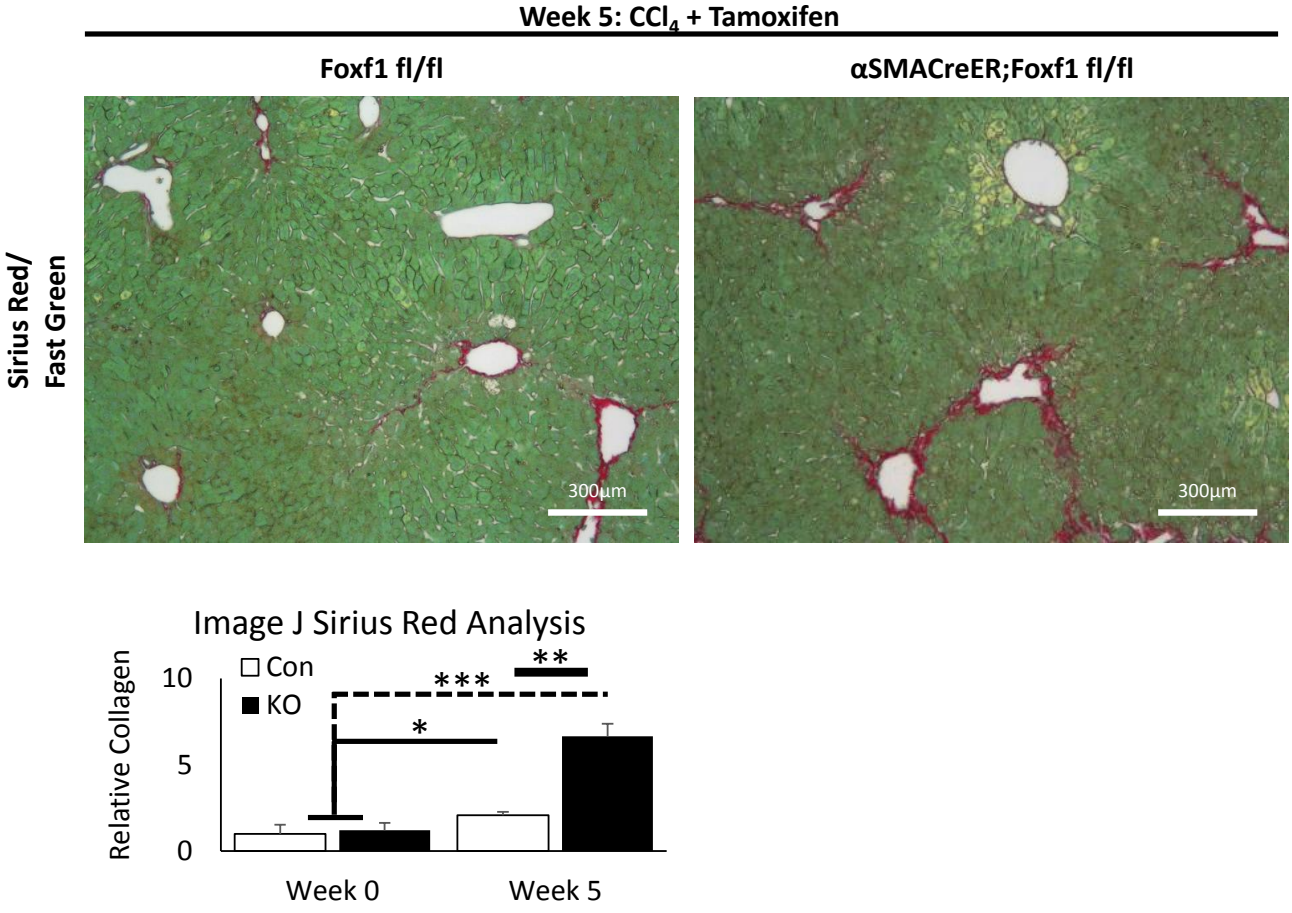

Figure S4. Increased collagen deposition in Foxf1*-deficient livers.* Sirius Red/Fast Green staining shows widespread collagen accumulation in *αSMACreER;Foxf1*$^{-/-}$ livers compared to *Foxf1*$^{fl/fl}$ livers. ImageJ analysis of Sirius Red/Fast Green images shows a significant increase in collagen in livers from *αSMACreER;Foxf1*$^{-/-}$ mice. n=3 mice for Con and n=4 mice for KO in week 0; n=4 mice for Con and n=5 mice for KO in week 5. P<0.05 is indicated with *, P<0.01 is indicated with **, P<0.001 is indicated with ***.

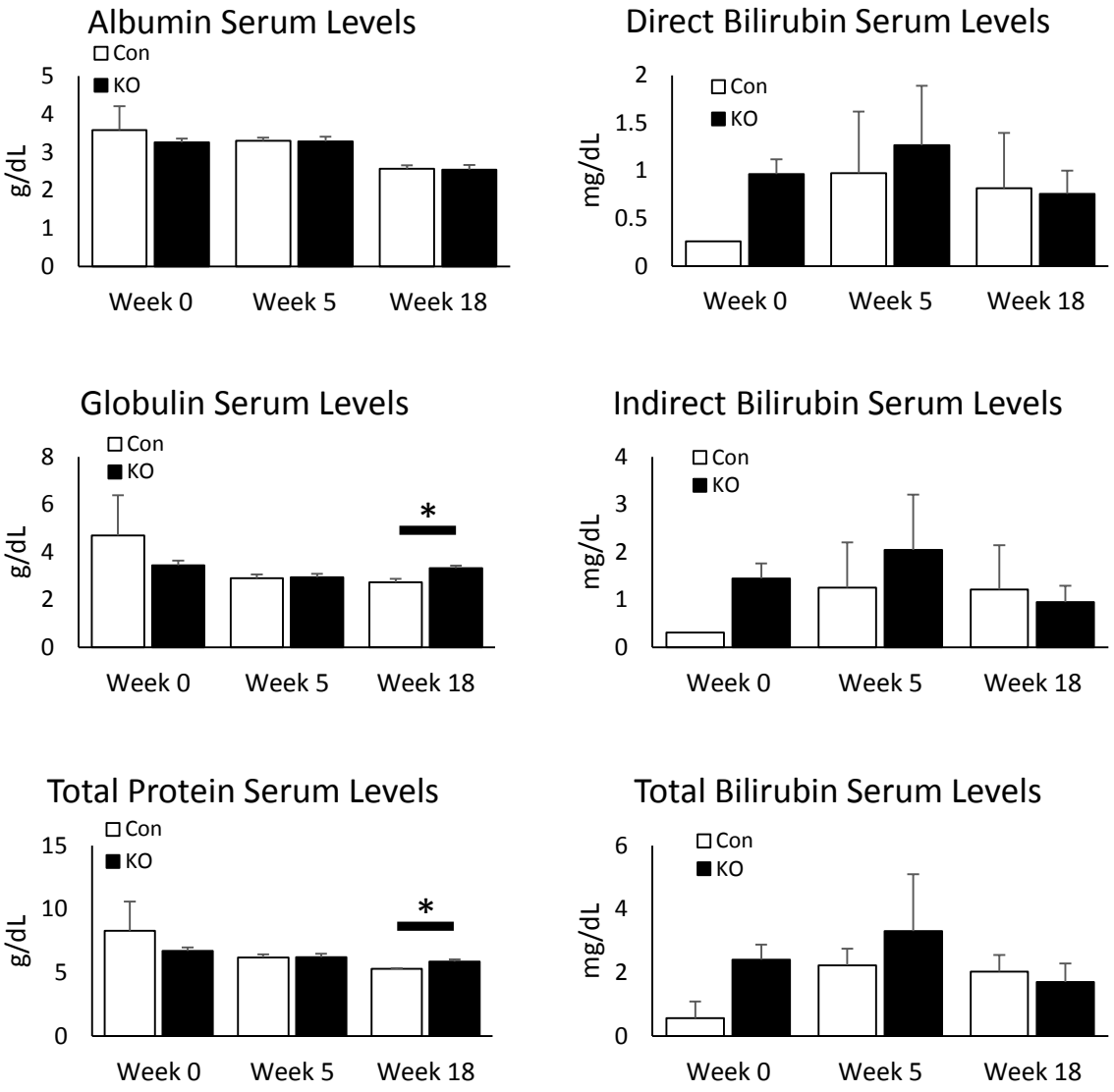

Figure S5. Deletion of Foxf1 *had no effect on serum protein or bilirubin levels.* The loss of *Foxf1* did not change serum albumin levels between control and *Foxf1*-deficient mice at 0, 5, or 18 weeks of CCl_4-treatment. Globulin levels were significantly increased at week 18 between *Foxf1*$^{fl/fl}$ and *αSMACreER;Foxf1*$^{-/-}$ livers, as were total protein levels. n=5 mice per group in weeks 0 and 5; n=3 control mice and n=5 KO mice in week 18. Deletion of *Foxf1* had no effect on bilirubin levels in blood serum. Data are shown as mean ± SEM.

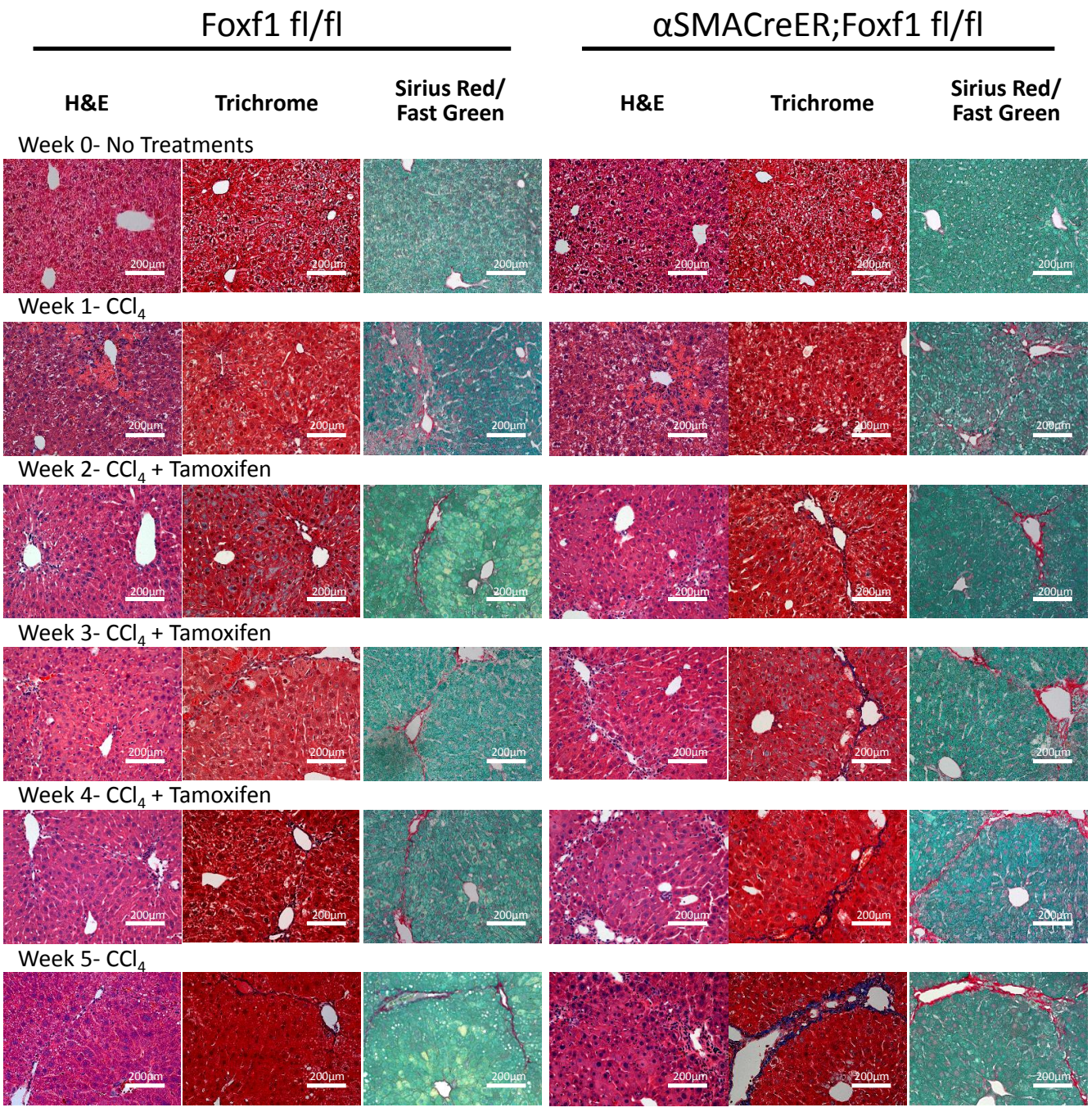

Figure S6. Collagen accumulation in Foxf1*-deficient livers is time-dependent.* H&E, Masson's trichrome, and Sirius Red/Fast green staining show a timecourse of CCl_4-induced hepatic fibrosis. Collagen depositions were greater in CCl_4-treated *αSMACreER;Foxf1*$^{-/-}$ livers.

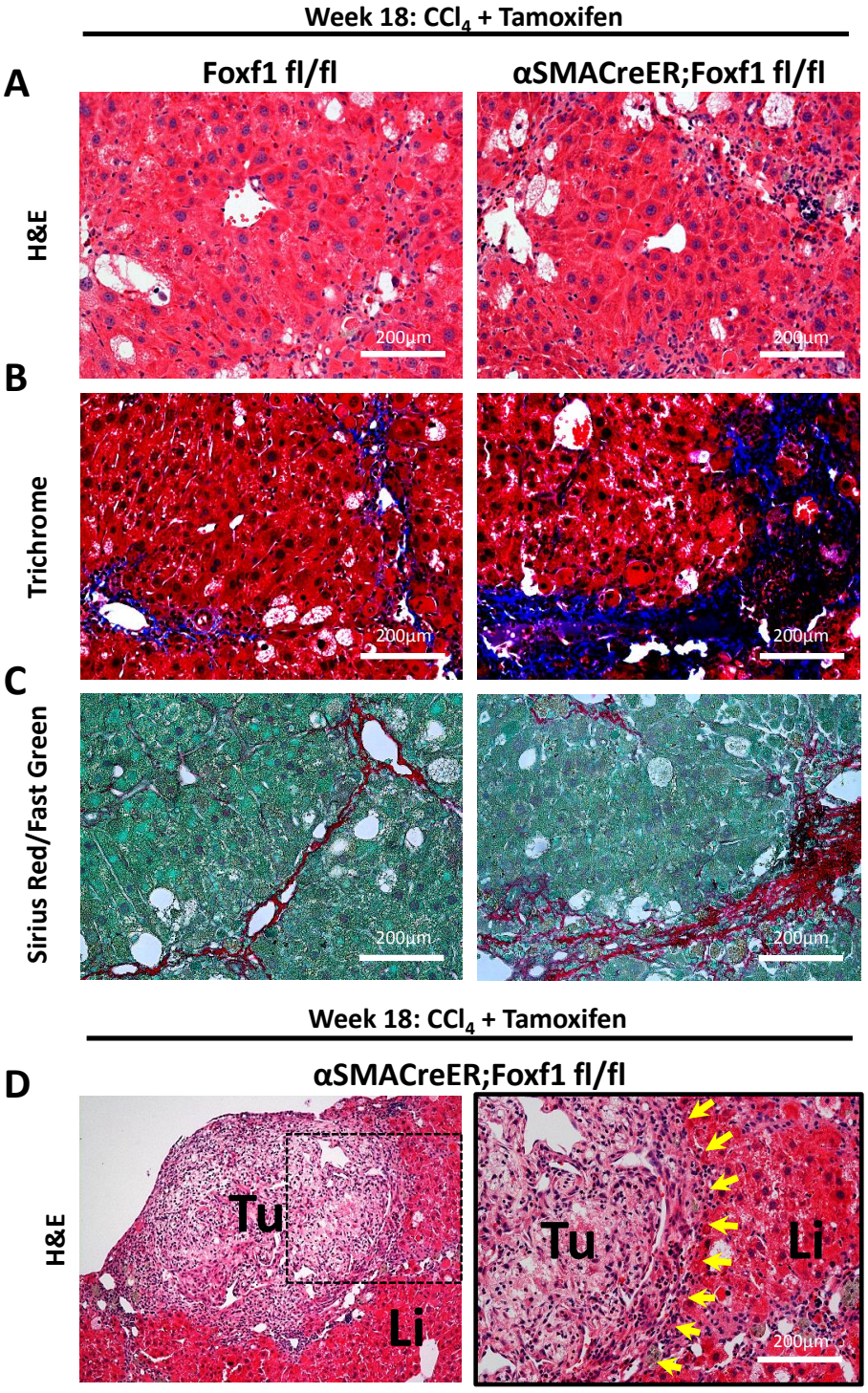

Figure S7. Widespread hepatic fibrosis and appearance of liver tumor in αSMACreER;Foxf1$^{-/-}$ *mouse after 18-weeks of* CCl_4 *treatment.* Representative liver sections stained for (A) H&E, (B) Masson's Trichrome, and (C) Sirius Red/Fast Green demonstrate that severe fibrotic lesions occur in *αSMACreER;Foxf1*$^{-/-}$ livers after 18-weeks of chronic hepatic injury. (D) H&E images show a hepatic tumor (Tu) in an *αSMACreER;Foxf1*$^{-/-}$ liver (Li) after 18-weeks of CCl_4-treatment. Tumors were found in 14.29% of mice (1 mouse out of n=7). Tumor boundaries are shown with arrows.

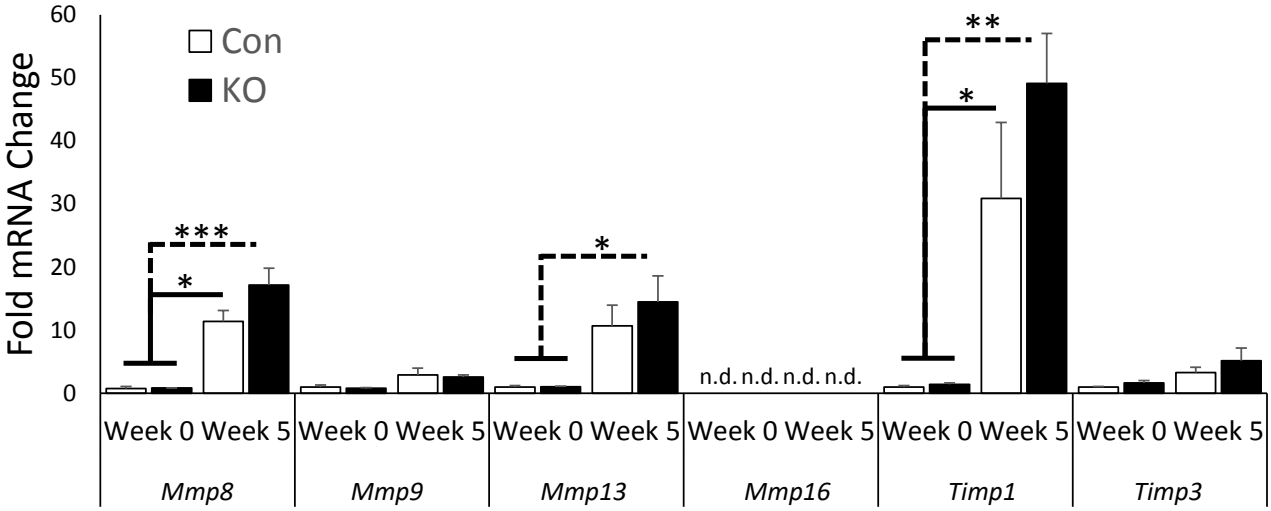

Figure S8. Deletion of Foxf1 *does not affect* Mmp8, Mmp9, Mmp13, Mmp16, Timp1, *or* Timp3 *mRNAs in CCl_4-treated livers*. qRT-PCR was used to measure mRNAs in whole liver extract. *Mmp16* was not detected (n.d.) in any sample tested. mRNAs were normalized to *Actb*. For *Mmp8*, *Mmp9*, *Mmp13*, *Mmp16*, *Timp1*, and *Timp3*: n=3 mice per group in week 0; n=5 mice per group in week 5. $P<0.05$ is indicated with *, $P<0.01$ is indicated with **, $P<0.001$ is indicated with ***.

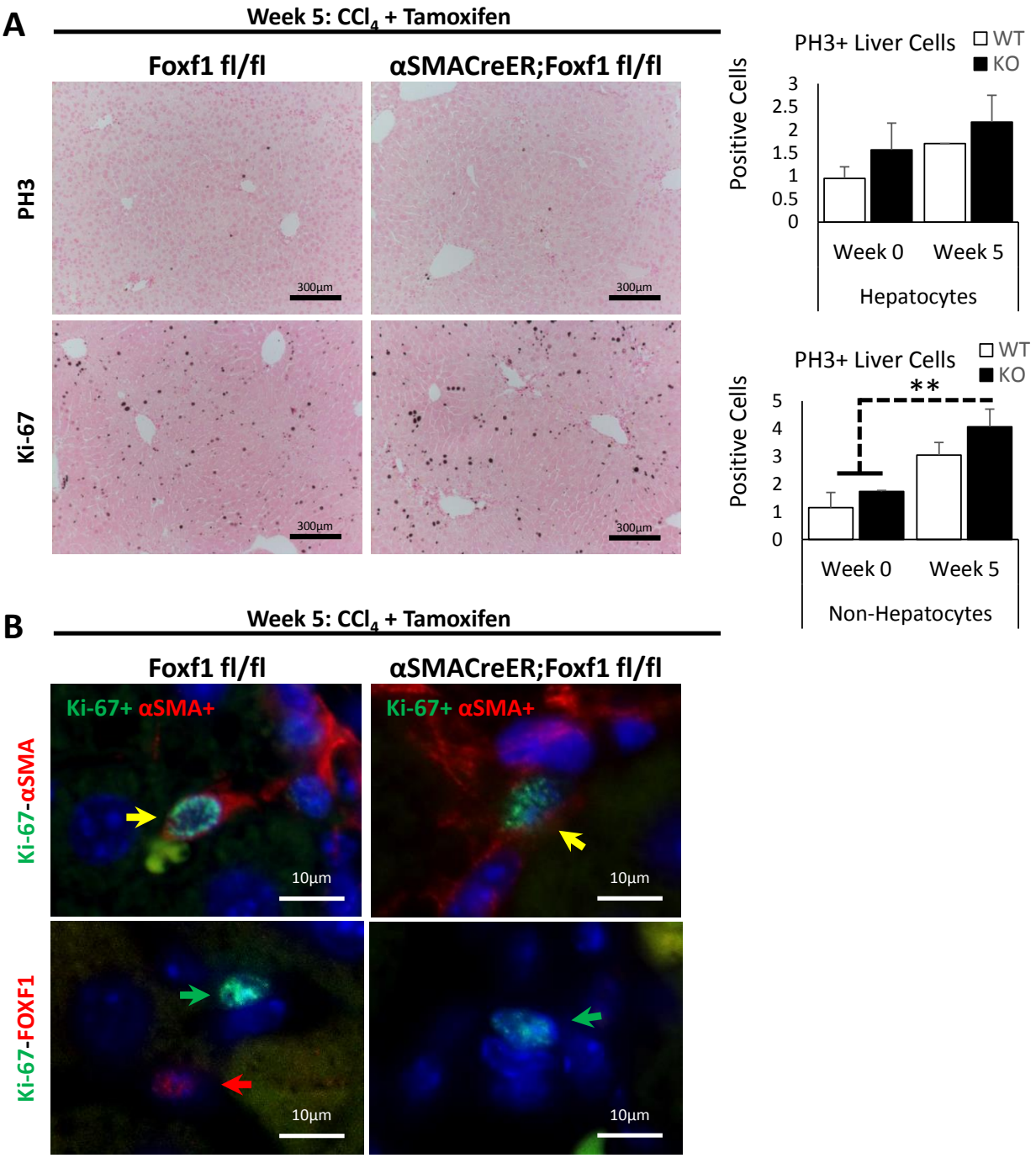

Figure S9. Deletion of Foxf1 *does not affect proliferation of* αSMA^{+} *cells in* CCl_4*-treated livers.* (A) Immunostaining for PH3 and Ki-67 and PH3 cell counts shows no difference between *Foxf1*$^{fl/fl}$ and *αSMACreER;Foxf1*$^{-/-}$ livers. The number of PH3^{+} hepatocytes and non-hepatocytes in *Foxf1*$^{fl/fl}$ livers was similar to those in *αSMACreER;Foxf1*$^{-/-}$ livers. Numbers of PH3^{+} cells were counted in 10 random 200x microscope fields using n=3 mice per group. (B) Co-localization of Ki-67 with αSMA shows the presence of Ki-67^{+} MFs in livers of CCl_4-treateed mice. Co-localization of Ki-67 with FOXF1 shows that proliferating FOXF1^{+} cells were uncommon in CCl_4-treated livers.

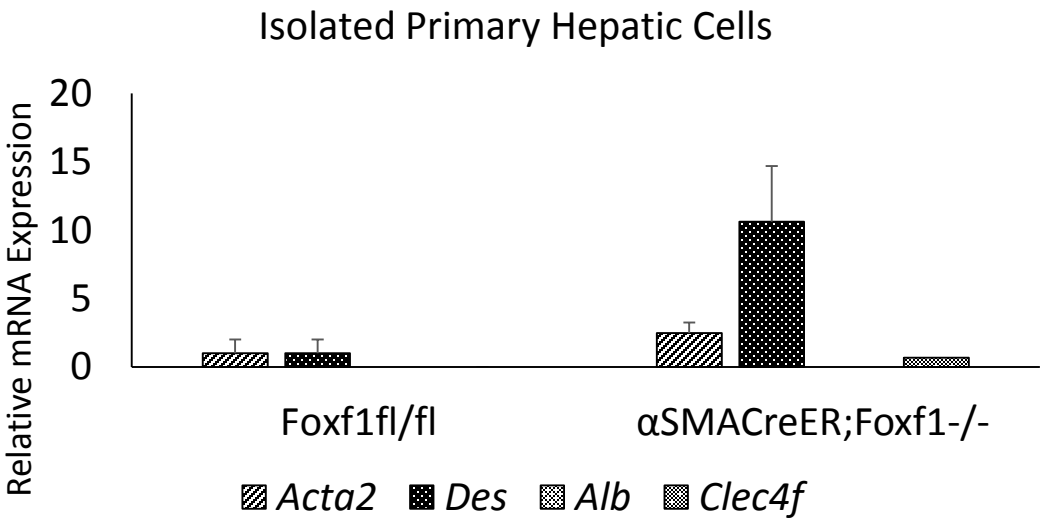

Figure S10. Purified stromal cells express Acta2 *and* Des. qRT-PCR analysis shows the presence of *Acta2* and *Des* mRNAs. Hepatocyte marker *Alb* and Kupffer cell marker *Clec4f* were not detected in purified stromal cells (one *αSMACreER;Foxf1*$^{-/-}$ sample expressed *Clec4f*). mRNAs were normalized to *Actb*.

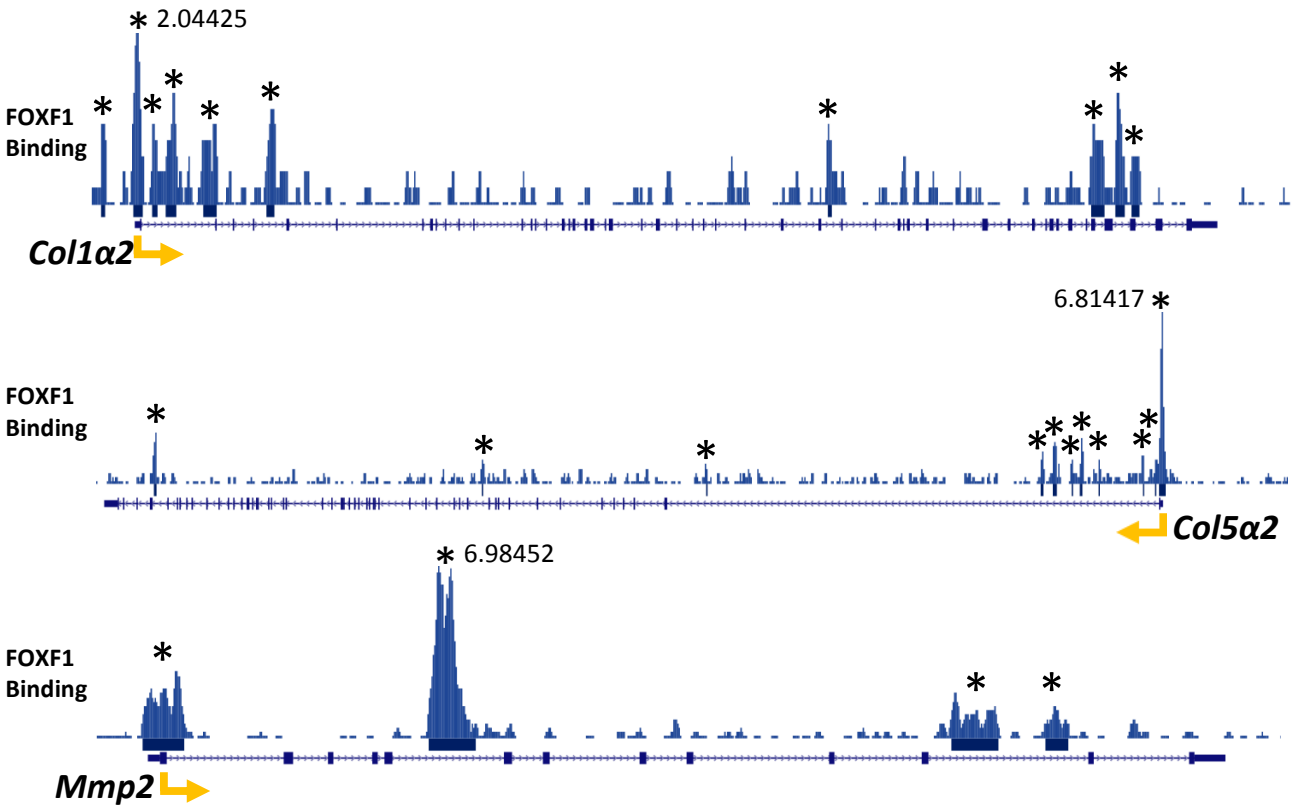

Figure S11. ChIP-seq shows FOXF1 binding sites in DNA regulatory regions of Col1α2, Col5α2, *and* Mmp2. Schematics of FOXF1 binding across entire genes: *Col1α2*, *Col5α2*, and *Mmp2*. ChIP-seq for FOXF1 shows significant binding in multiple DNA regions (indicated with *) of *Col1α2* (a peak binding height of 2.04425), *Col5α2* (a peak binding height of 6.81417), and *Mmp2* (a peak binding height of 6.98452).

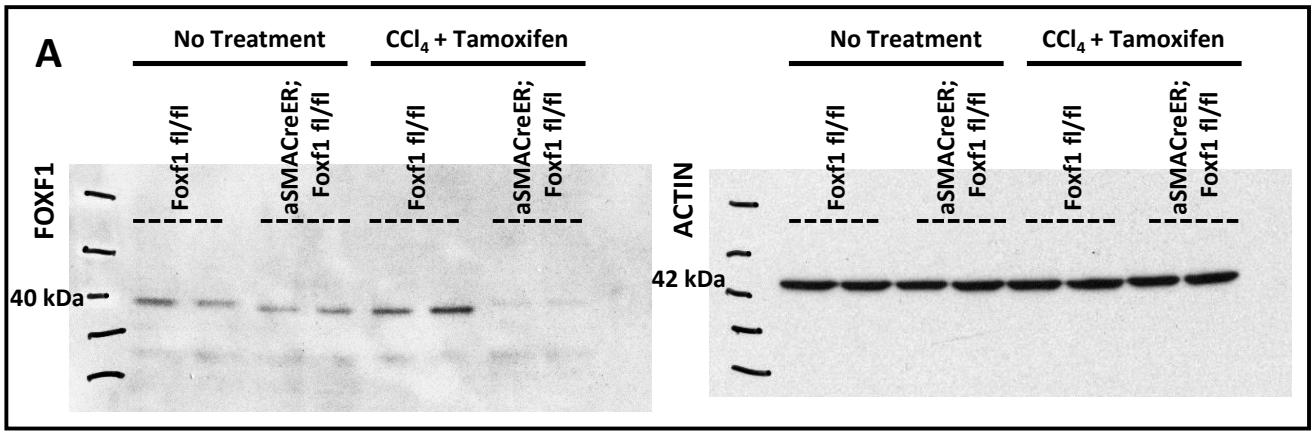

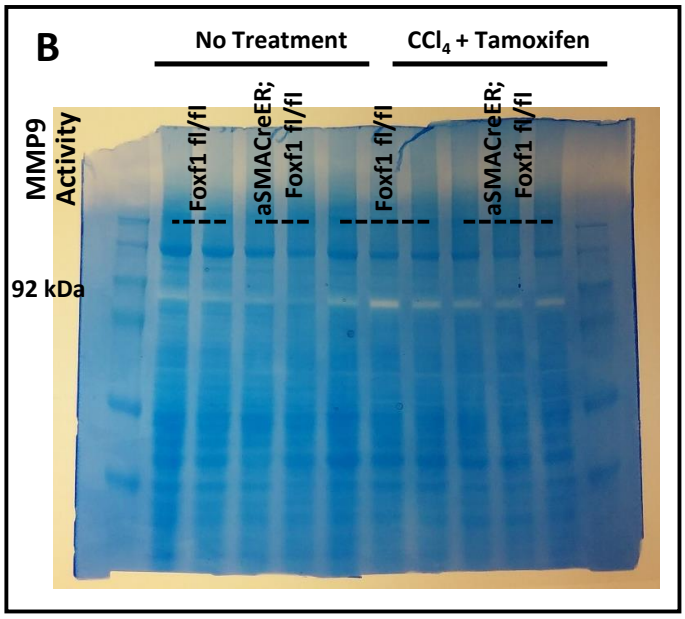

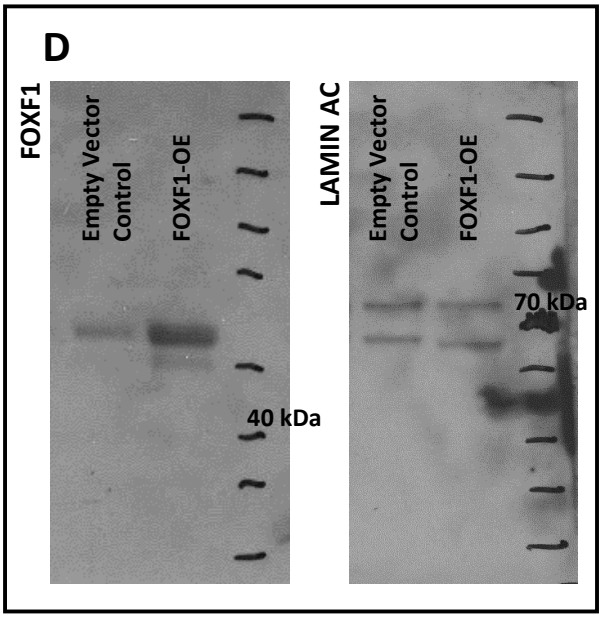

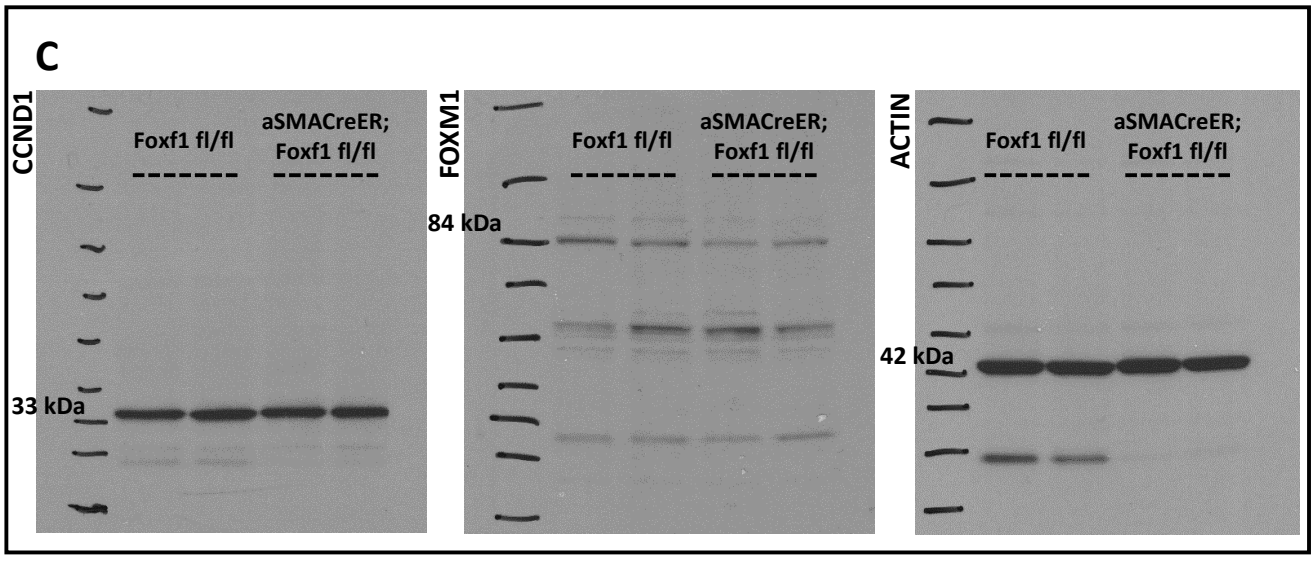

Figure S12. Full images for Western blot and zymography. (A) Full Western blots for FOXF1 (40 kDa) and corresponding ACTIN (42 kDa). Samples derive from the same experiment and blots were processed in parallel. Cropped blots are shown in Fig. 2C. (B) Full zymography gel used for analysis of MMP9 activity (92 kDa). Cropped gel shown in Fig. 3G. (C) Full Western blots for CCND1 (33 kDa), FOXM1 (84 kDa), and corresponding ACTIN (42 kDa). Samples derive from the same experiment and blots were processed in parallel. Cropped blots shown in Fig. 4G. (D) Full Western blots for FOXF1 and corresponding LAMIN AC (70 kDa). The FOXF1 bands are higher than the predicted 40 kDa due to the tags on the vector. Cropped blots shown in Fig. 6E.